

TWO MODELS FOR SURFACE SEGMENTATION USING THE TOTAL VARIATION OF THE NORMAL VECTOR

MANUEL WEISS, LUKAS BAUMGÄRTNER, LAURA WEIGL, RONNY BERGMANN,
STEPHAN SCHMIDT, AND ROLAND HERZOG

ABSTRACT. We consider the problem of surface segmentation, where the goal is to partition a surface represented by a triangular mesh. The segmentation is based on the similarity of the normal vector field to a given set of label vectors. We propose a variational approach and compare two different regularizers, both based on a total variation measure. The first regularizer penalizes the total variation of the assignment function directly, while the second regularizer penalizes the total variation in the label space. In order to solve the resulting optimization problems, we use variations of the split Bregman (ADMM) iteration adapted to the problem at hand. While computationally more expensive, the second regularizer yields better results in our experiments. In particular it removes noise more reliably in regions of constant curvature. In order to mitigate the computational cost, we present a manifold Newton scheme for the most expensive subproblem, which is related to the Riemannian center of mass on a sphere. This significantly improves the computational cost.

1. INTRODUCTION

Segmentation of surfaces is a fundamental task in computer vision and shape analysis. Its goal is to partition a given surface into disjoint regions based on certain features. In this paper, we consider surfaces that are represented by a mesh Γ consisting of a set \mathcal{T} of triangles and a set \mathcal{E} of edges in \mathbb{R}^3 . As the feature, we employ the unit outer normal vector field \mathbf{n} of the surface, which is piecewise constant. Segmentation then becomes the task of assigning a label to each triangle $T \in \mathcal{T}$, based on a measure of similarity of the triangle's normal vector \mathbf{n}_T to a set of prescribed label vectors $\mathbf{g}_1, \dots, \mathbf{g}_L$ belonging to the unit sphere $\mathcal{S} := \{\mathbf{x} \in \mathbb{R}^3 \mid |\mathbf{x}|_2 = 1\}$.

The result of a segmentation is expressed in terms of an assignment function $\varphi: \mathcal{T} \rightarrow \Delta$. Its value φ_T on each triangle T belongs to the probability simplex $\Delta := \{\mathbf{x} \in \mathbb{R}^L \mid \mathbf{1}^T \mathbf{x} = 1, \mathbf{x} \geq \mathbf{0}\}$. The label that will eventually be assigned to a triangle T is the one determined by the dominant entry in φ_T .

We follow a classical variational approach by minimizing a fidelity term that measures the similarity $s_\ell(\mathbf{n})$ of the normal vector \mathbf{n} to any of the label vectors \mathbf{g}_ℓ . We employ the geodesic distance d on the sphere \mathcal{S} for this purpose. That is, we

2010 *Mathematics Subject Classification.* 65D18, 68U10, 49M29, 65K05, 90C30.

Key words and phrases. total variation, surface segmentation, non-smooth optimization, ADMM, Newton's method.

This work was supported by DFG grants HE 6077/10-2 and SCHM 3248/2-2 within the Priority Program SPP 1962 (Non-smooth and Complementarity-based Distributed Parameter Systems: Simulation and Hierarchical Optimization), which is gratefully acknowledged.

have $s_\ell(\mathbf{n}) := d(\mathbf{n}, \mathbf{g}_\ell)$, which amounts to the angle between \mathbf{n} and \mathbf{g}_ℓ . These values can be pre-computed. We obtain the problem

$$(1.1) \quad \underset{\varphi: \mathcal{T} \rightarrow \Delta}{\text{Minimize}} \quad \sum_{T \in \mathcal{T}} |T| \sum_{\ell=1}^L s_\ell(\mathbf{n}_T) \varphi_{T,\ell} + \beta \mathcal{R}(\varphi).$$

In (1.1), $|T|$ denotes the area of T , $\beta > 0$ is a regularization parameter and \mathcal{R} is a regularizing functional.

The goal of this paper is to compare two regularization approaches, one of which is new in surface segmentation problems. The first regularizer was originally proposed for image segmentation problems in [Lellmann, Kappes, et al., 2009](#) and further developed in [Lellmann, Schnörr, 2011](#); [He et al., 2012](#). It measures the total variation of the assignment function φ in the assignment simplex Δ , and thus we refer to it as *assignment space total variation*, or A-TV in short. The variational problem (1.1) at hand has the same structure as in [Lellmann, Kappes, et al., 2009](#), but the pixels of the image domain are replaced by the triangles of the surface mesh and their color or gray-scale values are replaced by the normal vector data.

A drawback of A-TV is that it does not incorporate any metric structure in the space of labels. Any transition of the labels assigned to neighboring triangles is penalized by equal amounts, regardless of the distance between the labels. For the purpose of comparison with A-TV, we therefore propose an alternative regularizer, which measures the total variation in the label space \mathcal{S} instead. This means that incremental variations of the normal vector along a geodesic path on the sphere will be penalized no more than a single jump between the end points of that path. We refer to this new approach as *label space total variation*, or L-TV in short.

We can expect that L-TV will allow for smoother assignments, e. g., in regions of constant curvature, where neighboring normal vectors are close to each other. On the other hand, we acknowledge that L-TV is more involved computationally. This is primarily due to the fact that any value of the assignment function φ_T that is not a vertex of the simplex Δ corresponds to a mixture of labels. Due to the nonlinearity of the sphere \mathcal{S} as a space, this mixture is not simply a convex combination but rather a nonlinear weighted average known as the Riemannian center of mass; see [Karcher, 1977](#).

The Riemannian center of mass problem is a prominent optimization problem on Riemannian manifolds. A variant of it appears as a subproblem in the algorithm we propose to minimize the L-TV model. In order to mitigate the computational cost of this expensive step, we present a novel Newton scheme based on [Weigl, Schiela, 2024](#) that solves these subproblems more efficiently than gradient descent in our setting.

Related Literature. We briefly discuss alternative approaches to surface segmentation different from A-TV and L-TV. In [Wu et al., 2012](#), the authors consider a variational model similar to A-TV but with the squared distance as similarity measure $s_\ell(\mathbf{n}) := d(\mathbf{n}, \mathbf{g}_\ell)^2$. In [Lellmann, Schnörr, 2011](#), the authors use so-called interaction potentials to achieve a similar effect as the label space total-variation (L-TV) regularizer studied below. The interaction potentials allow for different penalization of label-jumps. The method proposed in [Hwan Kim, Dong Yun, Uk Lee, 2006](#); [Wang, Yu, 2011](#) iteratively merges triangles into larger regions, also using the outer normal vector field as a feature. Furthermore, [Sun, Harik, Baek, 2018](#); [Gauthier et al., 2017](#); [Yamauchi et al., 2005](#) compute an assignment based

on discrete notions of mesh curvature, derived from the normal vector \mathbf{n} . In an alternative variational approach, Cohen-Steiner, Alliez, Desbrun, 2004; Yan et al., 2012 achieve segmentation by minimizing the distance of the given mesh to an idealized mesh associated with the segmentation. The authors in Nabi, Douik, 2016; Zhang, Zheng, et al., 2012; Zhang, Wu, et al., 2017 propose a segmentation approach based on minimizing the Mumford-Shah functional Mumford, Shah, 1989, which is well-known from imaging applications. Finally, there is a stream of literature in geometric and topological data science, in which neural networks are trained to perform the task of surface segmentation or related inverse shape problems; see, e. g., Hanocka et al., 2019; Charles et al., 2017.

Contributions. We investigate two total-variation regularizers for surface segmentation problems based on the normal vector field as a feature. The *assignment space total variation* regularizer (A-TV) is a straightforward adaptation from image to surface segmentation. The *label space total variation* (L-TV) also borrows ideas previously used for manifold-valued imaging segmentation but appears to be new in the context of surface segmentation. It takes into account the metric structure of the label space, i. e., the unit sphere since we use the normal vector as feature. We develop an Alternating Direction Method of Multipliers (ADMM) approach to solve L-TV problems. In particular, we present a novel Newton scheme — an algorithm that may be of independent interest — for problems closely related to the Riemannian center of mass arising in every ADMM iteration. We compare the segmentation results obtained by A-TV and L-TV in numerical experiments that demonstrate that the L-TV model may yield smoother assignment functions, albeit at higher computational cost.

Outline. This paper is structured as follows: Section 2 introduces the required notions on triangulated surfaces and differential geometry of the sphere \mathcal{S} and the probability simplex Δ . In Section 3, we define the A-TV and L-TV models and discuss their differences. Section 4 presents algorithms to solve each problem numerically. This specifically includes a new manifold Newton scheme for one of the subproblems of the L-TV model that is related to the Riemannian center of mass. Section 5 presents numerical results that allow A-TV to be compared to L-TV.

2. PRELIMINARIES

2.1. Discrete Surfaces. In this work, we consider triangulated surface meshes Γ that are embedded in \mathbb{R}^3 . We denote the set of triangles by \mathcal{T} and the set of edges by \mathcal{E} . We work with manifold meshes without boundary, i. e., we assume that every edge E is connected to exactly two triangles. The two sides of an edge are denoted by E_+ and E_- , respectively, with arbitrary but fixed orientation. Furthermore, we assume that the surface is oriented, i. e., there exists a global outer unit normal vector field \mathbf{n} .

On the mesh Γ , we define the space of piecewise constant, X -valued functions

$$\mathcal{DG}(\mathcal{T}, X) := \{\mathbf{u}: \mathcal{T} \rightarrow X \mid \mathbf{u}|_T \in P_0(T, X) \text{ for all } T \in \mathcal{T}\}.$$

Here, $P_0(T, X)$ denotes the space of constant functions on the triangle T with values in X . For instance, the fact that the unit normal vector field \mathbf{n} is piecewise constant and has values on the sphere can be expressed as $\mathbf{n} \in \mathcal{DG}(\mathcal{T}, \mathcal{S})$.

On the skeleton (the union of edges), we analogously define

$$\mathcal{DG}(\mathcal{E}, X) := \{\mathbf{u}: \mathcal{E} \rightarrow X \mid \mathbf{u}|_E \in P_0(E, X) \text{ for all } E \in \mathcal{E}\}.$$

We denote the constant value of \mathbf{u} on a triangle T by $\mathbf{u}_T := \mathbf{u}|_T$ for $\mathbf{u} \in \mathcal{DG}(\mathcal{T}, X)$. Analogously, we write $\mathbf{u}_E := \mathbf{u}|_E$ for $\mathbf{u} \in \mathcal{DG}(\mathcal{E}, X)$.

2.2. Differential Geometry on the Sphere. Given a point $\mathbf{m} \in \mathcal{S}$, we denote its tangent plane by $\mathcal{T}_\mathbf{m}\mathcal{S}$. The tangent bundle \mathcal{TS} is the disjoint union of all tangent planes, endowed with the smooth structure inherited from \mathcal{S} . We choose the Euclidean inner product from the embedding $\mathcal{T}_\mathbf{m}\mathcal{S} \subseteq \mathbb{R}^3$ as the Riemannian metric on \mathcal{S} , turning the sphere into a Riemannian manifold. We denote the norm of a tangent vector by $|\cdot|_2$. The exponential map describes the point on the sphere reached by following the geodesic starting at $\mathbf{m} \in \mathcal{S}$ in tangential direction \mathbf{X} for unit time. It is explicitly given by

$$\exp_\mathbf{m}: \mathcal{T}_\mathbf{m}\mathcal{S} \rightarrow \mathcal{S}, \quad \mathbf{X} \mapsto \exp_\mathbf{m} \mathbf{X} = \cos(|\mathbf{X}|_2) \mathbf{m} + \sin(|\mathbf{X}|_2) \frac{\mathbf{X}}{|\mathbf{X}|_2},$$

see for instance the appendix of [Bergmann et al., 2020b](#) or [Boumal, 2023](#), Exercise 10.38. The inverse mapping $\log_\mathbf{m}$ is well-defined except on pairs of antipodal points. It satisfies

$$\exp_\mathbf{m}(\log_\mathbf{m}(\widetilde{\mathbf{m}})) = \widetilde{\mathbf{m}} \quad \text{for } \widetilde{\mathbf{m}} \neq -\mathbf{m}.$$

The parallel transport $P_{\widetilde{\mathbf{m}} \leftarrow \mathbf{m}}: \mathcal{T}_\mathbf{m}\mathcal{S} \rightarrow \mathcal{T}_{\widetilde{\mathbf{m}}}\mathcal{S}$ transports a tangent vector at \mathbf{m} to a tangent vector $\mathbf{X} \in \mathcal{T}_\mathbf{m}\mathcal{S}$ at $\widetilde{\mathbf{m}}$ along the unique shortest geodesic from \mathbf{m} to $\widetilde{\mathbf{m}} \neq -\mathbf{m}$. The parallel transport has the following explicit representation,

$$(2.1) \quad P_{\widetilde{\mathbf{m}} \leftarrow \mathbf{m}}(\mathbf{X}) = \mathbf{X} - 2 \frac{\mathbf{X}^\top (\mathbf{m} + \widetilde{\mathbf{m}})}{|\mathbf{m} + \widetilde{\mathbf{m}}|_2^2} (\mathbf{m} + \widetilde{\mathbf{m}}),$$

where $\mathbf{m}, \widetilde{\mathbf{m}} \in \mathcal{S}$ and again $\widetilde{\mathbf{m}} \neq -\mathbf{m}$ is required.

The choice of the Riemannian metric, i. e., the family of inner products in the tangent spaces $\mathcal{T}_\mathbf{m}\mathcal{S}$, induces a notion of distance on \mathcal{S} . For two points $\widetilde{\mathbf{m}}, \mathbf{m} \in \mathcal{S}$, the geodesic distance agrees with the ‘‘great arc distance’’

$$(2.2) \quad d_\mathcal{S}(\widetilde{\mathbf{m}}, \mathbf{m}) = \arccos(\widetilde{\mathbf{m}} \cdot \mathbf{m}) = \sphericalangle(\widetilde{\mathbf{m}}, \mathbf{m}),$$

where $\sphericalangle(\widetilde{\mathbf{m}}, \mathbf{m})$ denotes the angle (arc-length). As on any Riemannian manifold, the geodesic distance is related to the logarithmic map via

$$(2.3) \quad d_\mathcal{S}(\widetilde{\mathbf{m}}, \mathbf{m}) = |\log_\mathbf{m}(\widetilde{\mathbf{m}})|_2,$$

whenever the latter is defined; see also [Goto, Sato, 2021](#). The logarithmic map on the sphere \mathcal{S} is given by

$$(2.4) \quad \log_\mathbf{m}(\widetilde{\mathbf{m}}) = \begin{cases} \mathbf{0} & \text{if } \widetilde{\mathbf{m}} = \mathbf{m}, \\ \arccos(\widetilde{\mathbf{m}} \cdot \mathbf{m}) \frac{\widetilde{\mathbf{m}} - (\mathbf{m} \cdot \widetilde{\mathbf{m}}) \mathbf{m}}{|\widetilde{\mathbf{m}} - (\mathbf{m} \cdot \widetilde{\mathbf{m}}) \mathbf{m}|_2} & \text{otherwise,} \end{cases}$$

where again the case $\widetilde{\mathbf{m}} = -\mathbf{m}$ is excluded. It is worth noting that using (2.3) over (2.2) provides considerably more information about the structure of the non-smoothness of the problem. It is well known that $\widetilde{\mathbf{m}} \mapsto \log_\mathbf{m}(\widetilde{\mathbf{m}})$ is a smooth function in particular at $\widetilde{\mathbf{m}} = \mathbf{m}$. Hence the non-smoothness of (2.2) stems solely from the non-differentiability of the norm $|\cdot|_2$ at the tangent’s space origin.

For the Newton scheme we devise in [Section 4.2.4](#), we will need second derivatives of the logarithmic map (2.4). To this end, we state the following result whose proof is straightforward. We rewrite $\log_\mathbf{m}(\widetilde{\mathbf{m}}) = h(\widetilde{\mathbf{m}} \cdot \mathbf{m}) (\widetilde{\mathbf{m}} - (\mathbf{m} \cdot \widetilde{\mathbf{m}}) \mathbf{m})$, where

$$(2.5) \quad h: (-1, 1] \rightarrow \mathbb{R}, \quad h(x) = \begin{cases} \frac{\arccos(x)}{\sqrt{1-x^2}} & \text{if } x < 1, \\ 1, & \text{else.} \end{cases}$$

The derivatives of h for $x \in (-1, 1]$ are given by

$$(2.6a) \quad h'(x) = \frac{1}{(1-x^2)^{3/2}} (x \arccos(x) - \sqrt{1-x^2}),$$

$$(2.6b) \quad h''(x) = \frac{1}{(1-x^2)^{5/2}} (\arccos(x)(1+2x^2) - 3x\sqrt{1-x^2}).$$

In particular, we have

$$(2.7) \quad \lim_{x \rightarrow 1^-} h(x) = 1, \quad \lim_{x \rightarrow 1^-} h'(x) = -\frac{1}{3}, \quad \lim_{x \rightarrow 1^-} h''(x) = \frac{4}{15}.$$

We further recall the *Riemannian center of mass*, a generalization of the Euclidean mean on manifolds, as proposed by [Karcher, 1977](#). Given L points $\mathbf{g}_\ell \in \mathcal{S}$, $\ell = 1, \dots, L$ and corresponding weights $\varphi_\ell \in \mathbb{R}_{\geq 0}$, a point $\mathbf{m} \in \mathcal{S}$ is said to be a Riemannian center of mass w.r.t. the data $(\varphi_\ell, \mathbf{g}_\ell)$ if

$$(2.8) \quad \mathbf{m} \in \arg \min_{\mathbf{m} \in \mathcal{S}} \sum_{\ell=1}^L \varphi_\ell d_{\mathcal{S}}(\mathbf{m}, \mathbf{g}_\ell)^2.$$

In general, there is no closed-form solution to compute such \mathbf{m} . However, if a Riemannian center of mass \mathbf{m} fulfills $\mathbf{m} \neq -\mathbf{g}_\ell$ for all $\ell = 1, \dots, L$, the necessary optimality condition reads

$$(2.9) \quad 0 = \sum_{\ell=1}^L \varphi_\ell \log_{\mathbf{m}}(\mathbf{g}_\ell).$$

Notice that in Euclidean space, rather than the sphere, $\log_{\mathbf{m}}(\mathbf{g}_\ell) = \mathbf{g}_\ell - \mathbf{m}$ holds and thus (2.9) amounts to $\mathbf{m} = (\sum_{\ell=1}^L \varphi_\ell \mathbf{g}_\ell) / (\sum_{\ell=1}^L \varphi_\ell)$, thus explaining why the Riemannian center of mass generalizes the Euclidean mean.

For $\mathbf{m} \in \mathcal{DG}(\mathcal{T}, \mathcal{S})$, we further define

$$\begin{aligned} \mathcal{DG}(\mathcal{T}, \mathcal{TS}, \mathbf{m}) &:= \{\mathbf{Y} \in \mathcal{DG}(\mathcal{T}, \mathcal{TS}) \mid \mathbf{Y}_T \in \mathcal{T}_{\mathbf{m}_T} \mathcal{S} \text{ for all } T \in \mathcal{T}\}, \\ \mathcal{DG}(\mathcal{E}, \mathcal{TS}, \mathbf{m}) &:= \{\mathbf{X} \in \mathcal{DG}(\mathcal{E}, \mathcal{TS}) \mid \mathbf{X}_E \in \mathcal{T}_{\mathbf{m}_{E^+}} \mathcal{S} \text{ for all } E \in \mathcal{E}\}. \end{aligned}$$

2.3. Differential Geometry on the Simplex. In addition to the closed probability simplex

$$\Delta = \{\varphi \in \mathbb{R}^L \mid \mathbf{1}^\top \varphi = 1, \varphi \geq \mathbf{0}\},$$

we also require the open probability simplex

$$\tilde{\Delta} := \{\varphi \in \mathbb{R}^L \mid \mathbf{1}^\top \varphi = 1, \varphi > \mathbf{0}\}.$$

The tangent space $\mathcal{T}_\varphi \tilde{\Delta}$ at any point $\varphi \in \tilde{\Delta}$ is given by

$$\mathcal{T}_\varphi \tilde{\Delta} = \{\mathbf{X} \in \mathbb{R}^L \mid \mathbf{1}^\top \mathbf{X} = 0\}.$$

Using the Fisher-Rao metric, $\tilde{\Delta}$ can be equipped with a Riemannian manifold structure; see, e.g., [Åström et al., 2017](#), Sec. 2.1 for details. The geodesic distance

increases compared to the Euclidean distance close to the boundary. Given a point $\varphi \in \tilde{\Delta}$, the exponential map $\exp_\varphi: \mathcal{T}_\varphi \tilde{\Delta} \rightarrow \tilde{\Delta}$ is given by

$$(2.10) \quad \exp_\varphi(\mathbf{X}) = \frac{1}{2} \left(\varphi + \frac{\mathbf{X}_\varphi^2}{|\mathbf{X}_\varphi|^2} \right) + \frac{1}{2} \left(\varphi - \frac{\mathbf{X}_\varphi^2}{|\mathbf{X}_\varphi|^2} \right) \cos(|\mathbf{X}_\varphi|) + \frac{\sin(|\mathbf{X}_\varphi|)}{|\mathbf{X}_\varphi|} \mathbf{X}_\varphi \odot \sqrt{\varphi},$$

where $\mathbf{X}_\varphi = \mathbf{X}/\sqrt{\varphi}$ and $\odot, /, \sqrt{\cdot}$ are meant element-wise. Given a function $f: \mathbb{R}^L \rightarrow \mathbb{R}$ and a point $\varphi \in \tilde{\Delta}$, the Riemannian gradient $\text{grad}_{\tilde{\Delta}} f(\varphi)$ at φ can be computed using the Euclidean gradient $\nabla f(\varphi)$ by

$$(2.11) \quad \text{grad}_{\tilde{\Delta}} f(\varphi) = \nabla f(\varphi) \odot \varphi - (\varphi^T \nabla f(\varphi)) \varphi.$$

3. SEGMENTATION USING TWO TOTAL VARIATION REGULARIZERS

In this section, we discuss two regularizers \mathcal{R} for the segmentation problem (1.1): the *assignment space total variation* (A-TV) and the *label space total variation* (L-TV). We recall from (1.1) the common framework is to find a piecewise constant assignment function $\varphi \in \mathcal{DG}(\mathcal{T}, \Delta)$ that minimizes

$$\text{Minimize}_{\varphi \in \mathcal{DG}(\mathcal{T}, \Delta)} \sum_{T \in \mathcal{T}} |T| \sum_{\ell=1}^L s_\ell(\mathbf{n}_T) \varphi_{T,\ell} + \beta \mathcal{R}(\varphi).$$

In the absence of a regularizer ($\beta = 0$), the problem decouples and the minimum of $s_\ell(\mathbf{n}_T) \varphi_{T,\ell}$ is attained by the ℓ -th unit vector that corresponds to the label vector in $\{\mathbf{g}_1, \dots, \mathbf{g}_L\}$ that is closest to \mathbf{n}_T .

The purpose of the regularizer \mathcal{R} is to counteract noise in the normal vector data and achieve clean segmentation results. Both regularizers are based on the total variation for piecewise constant functions $\mathbf{u} \in \mathcal{DG}(\mathcal{T}, X)$ with values in a metric space (X, d_X) , defined as Bergmann et al., 2020a; Lellmann, Strekalovskiy, et al., 2013

$$(3.1) \quad \text{TV}_X(\mathbf{u}) := \sum_{E \in \mathcal{E}} |E| d_X(\mathbf{u}_{E_+}, \mathbf{u}_{E_-}),$$

where $|E|$ is the length of the edge E .

3.1. Segmentation Using Regularization by Assignment Space Total Variation. In a straightforward adaptation of Lellmann, Kappes, et al., 2009, we directly penalize the total variation of the assignment function φ . This corresponds to choosing $X = \Delta$ and $\mathbf{u} = \varphi$ and it leads to the *assignment space total variation* problem

$$(A-TV) \quad \text{Minimize}_{\varphi \in \mathcal{DG}(\mathcal{T}, \Delta)} \sum_{T \in \mathcal{T}} |T| \sum_{\ell=1}^L s_\ell(\mathbf{n}_T) \varphi_{T,\ell} + \beta \text{TV}_\Delta(\varphi).$$

We equip the simplex Δ with the metric induced by the 1-norm $|\cdot|_1$, so that the total variation term TV_Δ according to (3.1) becomes

$$(3.2) \quad \text{TV}_\Delta(\varphi) = \sum_{E \in \mathcal{E}} |E| |\varphi_{E_+} - \varphi_{E_-}|_1.$$

3.2. Segmentation Using Regularization by Label Space Total Variation.

As an alternative to (A-TV), we propose a second regularizer that is based on the total variation in the label space \mathcal{S} . Taking into account that the value of the assignment function φ in the simplex Δ represents a mixture of labels, we associate with φ a corresponding element $\mathbf{m}(\varphi)$ of the unit sphere \mathcal{S} . Since the latter is a nonlinear space, a mixture of these labels is not simply a convex combination but rather a nonlinear weighted average, the Riemannian center of mass (2.8). On the triangle T , this nonlinear mixture of the labels $\mathbf{g}_1, \dots, \mathbf{g}_L$ is given by

$$(3.3) \quad \mathbf{m}(\varphi)_T \in \arg \min_{\mathbf{m} \in \mathcal{S}} \sum_{\ell=1}^L \varphi_{T,\ell} d_{\mathcal{S}}(\mathbf{m}, \mathbf{g}_\ell)^2,$$

so that $\mathbf{m}(\varphi)$ is a piecewise constant function $\mathbf{m}(\varphi) \in \mathcal{DG}(\mathcal{T}, \mathcal{S})$. In terms of (3.1), the *label space total variation* problem corresponds to the choice $X = \mathcal{S}$ and $\mathbf{u} = \mathbf{m}(\varphi)$ and it reads

$$(L-TV) \quad \underset{\varphi \in \mathcal{DG}(\mathcal{T}, \Delta)}{\text{Minimize}} \quad \sum_{T \in \mathcal{T}} |T| \sum_{\ell=1}^L s_\ell(\mathbf{n}_T) \varphi_{T,\ell} + \beta \text{TV}_{\mathcal{S}}(\mathbf{m}(\varphi)).$$

In contrast to (3.2), the total variation term now considers the geodesic distances of neighboring Riemannian centers of mass,

$$(3.4) \quad \text{TV}_{\mathcal{S}}(\mathbf{m}(\varphi)) = \sum_{E \in \mathcal{E}} |E| d_{\mathcal{S}}(\mathbf{m}(\varphi)_{E_+}, \mathbf{m}(\varphi)_{E_-}).$$

Example 3.1 (Comparison of the regularizers). *To emphasize the difference of the alternative model (L-TV) compared to (A-TV), we compare the values of $\text{TV}_{\Delta}(\varphi)$ and $\text{TV}_{\mathcal{S}}(\mathbf{m}(\varphi))$ for two different assignments φ and $\tilde{\varphi}$. The situation is illustrated in Figure 3.1. Normalizing the edges where jumps occur to length one, we evaluate*

$$(3.5) \quad 2 = \text{TV}_{\Delta}(\varphi) < \text{TV}_{\Delta}(\tilde{\varphi}) = 4, \quad \text{TV}_{\mathcal{S}}(\mathbf{m}(\varphi)) = \text{TV}_{\mathcal{S}}(\mathbf{m}(\tilde{\varphi})) = \frac{\pi}{2}.$$

This clarifies that the assignment of an intermediate label between two assigned labels incurs an additional penalty in the assignment space total variation model (A-TV) but not in the (L-TV) model. This hints at the fact later confirmed by our numerical experiments that the (A-TV) model tends to “skip” labels to reduce the regularization penalty.

4. NUMERICAL ALGORITHMS

In this section, we present numerical methods for both models. The simpler assignment space total variation problem (A-TV) can actually be rewritten as a linear program with $(|\mathcal{T}| + |\mathcal{E}|) \cdot L$ variables, $2L \cdot |\mathcal{E}|$ inequality constraints and $|\mathcal{T}|$ equality constraints. In our largest problem instance (Section 5.2), this amounts to more than 1.4 million variables. While problems of this size, particularly with sparse constraint matrices, can be handled by state-of-the-art solvers, in this study we use the Chambolle-Pock algorithm Chambolle, Pock, 2011; Pock et al., 2009. This leads to very simple and parallelizable update steps.

The Chambolle-Pock method cannot be directly applied to the label space assignment problem (L-TV), because the Riemannian center of mass $\mathbf{m}(\varphi)$ does not depend linearly on the assignment φ . We therefore use an alternating direction

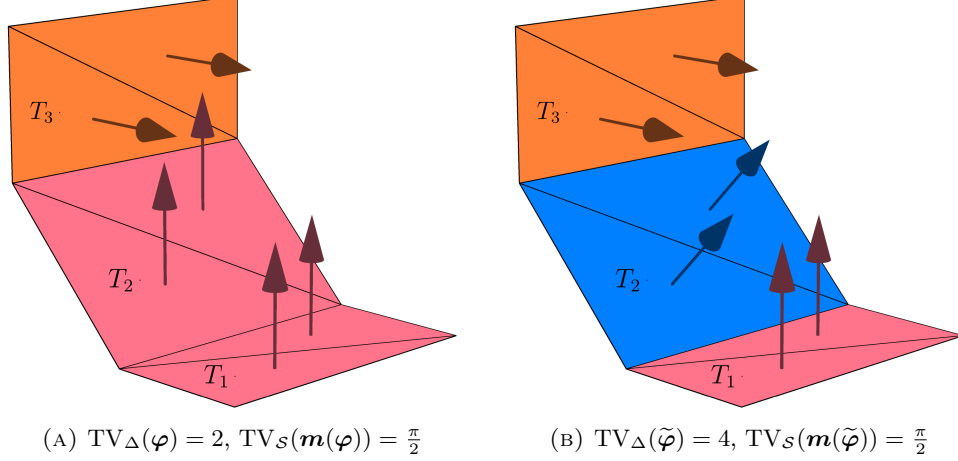


FIGURE 3.1. Visualization of the assignments $\varphi, \tilde{\varphi}$ as described in Theorem 3.1.

method of multipliers (ADMM) [Boyd et al., 2010](#), whose individual steps are also parallelizable and mostly simple.

4.1. Chambolle-Pock Algorithm for Assignment Space Total Variation.

For problem (A-TV), we use the Chambolle-Pock algorithm [Pock et al., 2009](#), similarly as in [Chambolle, Pock, 2011](#), Section 6.3.4. To set up the algorithm, we introduce the jump operator K

$$(4.1) \quad K: \mathcal{DG}(\mathcal{T}, \Delta) \rightarrow \mathcal{DG}(\mathcal{E}, \mathbb{R}^L), \quad (K\varphi)_E := \beta(\varphi_{E_+} - \varphi_{E_-}).$$

The algorithm can be written as shown in [Algorithm 1](#), where K^* denotes the Hilbert-space adjoint of K w.r.t. the L^2 -inner products on $\mathcal{DG}(\mathcal{T}, \mathbb{R}^L)$ and $\mathcal{DG}(\mathcal{E}, \mathbb{R}^L)$. These inner products are represented by diagonal matrices with the triangle areas or edge lengths on the diagonal, respectively.

Algorithm 1 Chambolle-Pock algorithm applied to the assignment space total variation problem (A-TV).

Input: similarity measure $\mathbf{s} \in \mathcal{DG}(\mathcal{T}, \mathbb{R}^L)$

Input: step sizes $\tau > 0, \sigma > 0$, extrapolation parameter $\theta \in [0, 1]$

Input: $\varphi^{(0)} \in \mathcal{DG}(\mathcal{T}, \Delta), \mathbf{v}^{(0)} \in \mathcal{DG}(\mathcal{E}, \mathbb{R}^L)$

Output: approximate solution of (A-TV)

- 1: Set $\tilde{\varphi}^{(0)} \leftarrow \varphi^{(0)}$
 - 2: **while** not converged **do**
 - 3: Set $\mathbf{v}_E^{(k+1)} \leftarrow \text{clip}(\mathbf{v}_E^{(k)} + \sigma[K\tilde{\varphi}^{(k)}]_E, -1, 1)$ for all edges E
 - 4: Set $\varphi_T^{(k+1)} \leftarrow \text{proj}_\Delta(\varphi_T^{(k)} - \tau[K^*\mathbf{v}^{(k+1)} - \tau\mathbf{s}]_T)$ for all triangles T
 - 5: Set $\tilde{\varphi}^{(k+1)} \leftarrow \varphi^{(k+1)} + \theta(\varphi^{(k+1)} - \varphi^{(k)})$
 - 6: $k \leftarrow k + 1$
 - 7: **end while**
-

Here, the clipping operator $\text{clip}(\cdot, -1, 1): \mathbb{R}^L \rightarrow [-1, 1]^L$ projects each component to the interval $[-1, 1]$. Further, the simplex projection proj_Δ in Algorithm 1 can be efficiently computed using Algorithm 1 in Wang, Carreira-Perpiñán, 2013.

We mention that (A-TV) can also be solved using other, potentially more efficient methods. For instance, one can rewrite it as a min-cut linear program and apply algorithms for this problem class; see, for instance, Yuan, Bae, Tai, 2010; Bae et al., 2014; Yuan, Bae, Tai, Boykov, 2010.

4.2. ADMM for Label Space Total Variation. Algorithm 1 cannot be transferred easily to the label space assignment problem (L-TV), because the Riemannian center of mass $\mathbf{m}(\varphi)$ does not depend linearly on the assignment φ . A method applicable to (L-TV) is the alternating direction method of multipliers (ADMM); see Boyd et al., 2010; Goldstein, Osher, 2009.

We now derive the specific form of that algorithm. In addition to the assignment variable $\varphi \in \mathcal{DG}(\mathcal{T}, \Delta)$, we introduce three auxiliary variables \mathbf{m} , \mathbf{Y} , and \mathbf{X} . As is customary in ADMM, the purpose of these variables is to allow problem (L-TV) to be split into simpler subproblems. Each of the auxiliary variables is coupled to the remaining variables through a constraint that is enforced by a penalty term in the augmented Lagrangian function.

The first auxiliary variable $\mathbf{m} \in \mathcal{DG}(\mathcal{T}, \mathcal{S})$ represents the Riemannian center of mass of the labels, weighted according to the assignment function φ per triangle. We introduce the necessary optimality condition (2.9) of the weighted Riemannian center of mass problem as the corresponding constraint. In fact, we replace the nonlinear terms $\log_{\mathbf{m}}(\mathbf{g}_\ell)$ in (2.9), triangle by triangle, by the auxiliary variable $\mathbf{Y} \in \mathcal{DG}(\mathcal{T}, \mathcal{TS})$. This leaves us with the constraint (2.9) in the form $\sum_{\ell=1}^L \varphi_{T,\ell} \mathbf{Y}_{T,\ell} = \mathbf{0}$ as well as $\mathbf{Y}_{T,\ell} = \log_{\mathbf{m}_T}(\mathbf{g}_\ell)$. For numerical stability, we represent the latter in the form $\mathbf{g}_\ell = \exp_{\mathbf{m}_T} \mathbf{Y}_{T,\ell}$.

Finally, to handle the non-smoothness in the total variation (3.4), we introduce the third auxiliary variable $\mathbf{X} \in \mathcal{DG}(\mathcal{E}, \mathcal{TS})$ coupled by the constraint $\mathbf{X}_E = \log_{\mathbf{m}_{E_+}}(\mathbf{m}_{E_-})$. We thus arrive at

$$(4.2) \quad \begin{array}{l} \underset{\varphi, \mathbf{m}, \mathbf{Y}, \mathbf{X}}{\text{Minimize}} \\ \text{subject to} \end{array} \quad \begin{cases} \sum_{T \in \mathcal{T}} |T| \varphi_T^T \mathbf{s}_T + \beta \sum_{E \in \mathcal{E}} |E| |\mathbf{X}_E|_2 \\ \mathbf{0} = \sum_{\ell=1}^L \varphi_{T,\ell} \mathbf{Y}_{T,\ell} \in \mathcal{T}_{\mathbf{m}_T} \mathcal{S} \quad \text{for all } T \in \mathcal{T}, \\ \mathbf{g}_\ell = \exp_{\mathbf{m}_T} \mathbf{Y}_{T,\ell} \in \mathcal{S} \subseteq \mathbb{R}^3 \quad \text{for all } T \in \mathcal{T}, \ell = 1, \dots, L, \\ \mathbf{X}_E = \log_{\mathbf{m}_{E_+}}(\mathbf{m}_{E_-}) \in \mathcal{T}_{\mathbf{m}_{E_+}} \mathcal{S} \quad \text{for all } E \in \mathcal{E}. \end{cases}$$

Notice that (4.2) is not strictly equivalent to (L-TV), because we use a necessary, but not sufficient, optimality condition to substitute the Riemannian center of mass \mathbf{m} . In practice, we did not observe any difficulties stemming from this discrepancy.

We associate with problem (4.2) the following augmented Lagrangian

$$\begin{aligned}
& \mathcal{L}_\rho(\boldsymbol{\varphi}, \mathbf{m}, \mathbf{Y}, \mathbf{X}, \boldsymbol{\lambda}, \boldsymbol{\mu}, \boldsymbol{\nu}) \\
&= \sum_{T \in \mathcal{T}} |T| \boldsymbol{\varphi}_T^\top \mathbf{s}_T + \beta \sum_{E \in \mathcal{E}} |E| \|\mathbf{X}_E\|_2 + \frac{\rho}{2} \sum_{T \in \mathcal{T}} |T| \left\| \sum_{\ell=1}^L \boldsymbol{\varphi}_{T,\ell} \mathbf{Y}_{T,\ell} + \boldsymbol{\lambda}_T \right\|_2^2 \\
&+ \frac{\rho}{2} \sum_{T \in \mathcal{T}} |T| \sum_{\ell=1}^L \|\exp_{\mathbf{m}_T}(\mathbf{Y}_{T,\ell}) - \mathbf{g}_\ell + \boldsymbol{\mu}_{T,\ell}\|_2^2 \\
(4.3) \quad &+ \frac{\rho}{2} \sum_{E \in \mathcal{E}} |E| \|\log_{\mathbf{m}_{E_+}}(\mathbf{m}_{E_-}) - \mathbf{X}_E + \boldsymbol{\nu}_E\|_2^2.
\end{aligned}$$

The quantities $\boldsymbol{\lambda} \in \mathcal{DG}(\mathcal{T}, \mathbb{R}^3)$, $\boldsymbol{\mu} \in \mathcal{DG}(\mathcal{T}, \mathbb{R}^{L \times 3})$, as well as $\boldsymbol{\nu} \in \mathcal{DG}(\mathcal{E}, \mathbb{R}^3)$ represent the (rescaled) Lagrange multipliers associated with the constraints in (4.2). The values of \mathbf{X} and \mathbf{Y} need to be constrained to belong to the respective tangent spaces of \mathcal{S} . Depending on \mathbf{m} , the same applies to $\boldsymbol{\lambda}$ and $\boldsymbol{\nu}$. This is addressed in for each variable separately in the following subsections.

In each iteration of ADMM, we subsequently minimize the augmented Lagrangian (4.3) with respect to one of the primal variables while fixing the others. We choose $\mathbf{Y}, \mathbf{X}, \boldsymbol{\varphi}, \mathbf{m}$ as the order of updates in order to best exploit the problem structure. Specifically, the \mathbf{Y} and \mathbf{X} problems turn out to be independent of each other, and likewise the $\boldsymbol{\varphi}$ and \mathbf{m} problems are independent of each other as well. We wish to point out that we did not encounter significant differences in the convergence behavior of the algorithm when changing the order of the updates.

We now address each of the four primal problems individually. The index $\cdot^{(k)}$ denotes the iteration number. The overall ADMM algorithm is described in Section 4.2.5.

4.2.1. The \mathbf{Y} -Subproblem. The minimization of (4.3) with respect to \mathbf{Y} decouples into independent smooth problems, one on each triangle T . Omitting the terms that do not depend on \mathbf{Y} as well as the factor $\frac{\rho}{2}|T|$ common to all remaining terms, we obtain

$$(4.4) \quad \underset{\mathbf{Y}_T \in (\mathcal{T}_{\mathbf{m}_T} \mathcal{S})^L}{\text{Minimize}} \quad \left\| \sum_{\ell=1}^L \boldsymbol{\varphi}_{T,\ell}^{(k)} \mathbf{Y}_{T,\ell} + \boldsymbol{\lambda}_T^{(k)} \right\|_2^2 + \sum_{\ell=1}^L \|\exp_{\mathbf{m}_T^{(k)}}(\mathbf{Y}_{T,\ell}) - \mathbf{g}_\ell + \boldsymbol{\mu}_{T,\ell}^{(k)}\|_2^2.$$

We solve these problems simultaneously by applying a (Euclidean) gradient descent scheme with an Armijo backtracking strategy in the space $\mathcal{DG}(\mathcal{T}, \mathcal{TS}, \mathbf{m})$. In fact, we check a stopping criterion per triangle and drop the converged triangles from subsequent gradient steps. As stopping criterion we use $|\nabla_{\mathbf{Y}_T} \mathcal{L}_\rho| \leq \max\{10^{-8}, 10^{-0.0025k}\}$, dependent on the iteration number k of the outer ADMM loop. The overall solution of the \mathbf{Y} -subproblem obtained in this way is denoted by $\mathbf{Y}_T^{(k+1)}$.

4.2.2. The \mathbf{X} -Subproblem. The minimization of (4.3) with respect to \mathbf{X} also decouples into independent problems, one on each edge E . Omitting the terms that do not depend on \mathbf{X} as well as the factor $|E|$ common to all remaining terms, we obtain

$$(4.5) \quad \underset{\mathbf{X}_E \in \mathcal{T}_{\mathbf{m}_{E_+}^{(k)}} \mathcal{S}}{\text{Minimize}} \quad \beta \|\mathbf{X}_E\|_2 + \frac{\rho}{2} \|\log_{\mathbf{m}_{E_+}^{(k)}}(\mathbf{m}_{E_-}^{(k)}) - \mathbf{X}_E + \boldsymbol{\nu}_E^{(k)}\|_2^2.$$

This problem is well known to have a closed-form solution in terms of a vector-valued soft-thresholding operation; see for instance [Goldstein, Osher, 2009](#). We obtain

$$(4.6) \quad \mathbf{X}_E^{(k+1)} = \left(1 - \frac{\beta/\rho}{\max\{\beta/\rho, |\log_{\mathbf{m}_{E_+}^{(k)}}(\mathbf{m}_{E_-}^{(k)}) + \boldsymbol{\nu}_E^{(k)}|_2\}} \right) \left(\log_{\mathbf{m}_{E_+}^{(k)}}(\mathbf{m}_{E_-}^{(k)}) + \boldsymbol{\nu}_E^{(k)} \right).$$

The result $\mathbf{X}_E^{(k+1)}$ is naturally an element of the tangent space $\mathcal{T}_{\mathbf{m}_{E_+}}\mathcal{S}$, because both $\log_{\mathbf{m}_{E_+}^{(k)}}(\mathbf{m}_{E_-}^{(k)})$ and $\boldsymbol{\nu}_E^{(k)}$ are.

4.2.3. *The $\boldsymbol{\varphi}$ -Subproblem.* Concerning $\boldsymbol{\varphi}$, the minimization of (4.3) decouples into independent quadratic programming problems (QPs), one on each triangle T . Omitting the terms that do not depend on $\boldsymbol{\varphi}$ as well as the factor $|T|$ common to all remaining terms, we obtain

$$(4.7) \quad \underset{\boldsymbol{\varphi}_T \in \Delta}{\text{Minimize}} \quad \boldsymbol{\varphi}_T^T \mathbf{s}_T + \frac{\rho}{2} \left| \sum_{\ell=1}^L \boldsymbol{\varphi}_{T,\ell} \mathbf{Y}_{T,\ell}^{(k+1)} + \boldsymbol{\lambda}_T^{(k)} \right|_2^2.$$

This is a standard convex QP with constraints $\boldsymbol{\varphi}^T \mathbf{1} = 0$ and $\boldsymbol{\varphi} \geq \mathbf{0}$. We initially solved these problems using the QP solver OSQP from [Stellato et al., 2020](#). However, we found that a specialized solver exploiting the geometry of the probability simplex can be more efficient, particularly in light of the fact that we need to solve one problem of type (4.7) for each triangle and each iteration of the ADMM algorithm, which may easily amount to millions of QPs solved. One such approach can be found in [Li, McKenzie, Yin, 2021](#), where the authors propose the substitution $\mathbf{z}_{T,\ell}^2 = \boldsymbol{\varphi}_{T,\ell}$ and solve the problem with $\mathbf{z} \in \mathcal{S}_L = \{\mathbf{x} \in \mathbb{R}^L \mid |\mathbf{x}|_2 = 1\}$ using the Riemannian manifold structure of the sphere. However, we propose the two-stage procedure described below, which exploits the fact that in later ADMM iterations the activity structure of the inequalities $\boldsymbol{\varphi}^{(k+1)} \geq \mathbf{0}$ is unchanged from the previous iterate $\boldsymbol{\varphi}^{(k)}$.

We proceed in a two-stage procedure to solve (4.7). In the first stage, we apply a Riemannian gradient descent scheme with an Armijo backtracking strategy on the open probability simplex $\tilde{\Delta}$. This makes use of the exponential map (2.10) and of the Riemannian gradient (2.11) of the objective in (4.7). The gradient scheme stops when the iterates approach the boundary, i. e., when a component $\boldsymbol{\varphi}_\ell$ becomes small, or when the norm of the Riemannian gradient falls below a threshold.

The approximate solution obtained in this way serves to determine the inactive and active inequalities, i. e., the subsets $\mathcal{I}, \mathcal{A} \subseteq \{1, \dots, L\}$, where $\boldsymbol{\varphi}_{T,\ell} = 0$ on \mathcal{A} . With the active set \mathcal{A} and its complement \mathcal{I} at hand, the KKT system for (4.7) becomes a linear system of equations,

$$(4.8) \quad \begin{aligned} \mathbf{0} &= \rho \mathbf{Y}_T \mathbf{Y}_T^T \boldsymbol{\varphi}_T + \rho \mathbf{Y}_T \boldsymbol{\lambda}_T + \mathbf{s}_T - \boldsymbol{\alpha}_T - \gamma_T \mathbf{1}, \\ 1 &= \mathbf{1}^T \boldsymbol{\varphi}_T, \\ 0 &= \boldsymbol{\varphi}_{T,\ell} \quad \text{for } \ell \in \mathcal{A}, \\ 0 &= \boldsymbol{\alpha}_{T,\ell} \quad \text{for } \ell \in \mathcal{I}. \end{aligned}$$

The variables $\boldsymbol{\alpha}_T \in \mathbb{R}^L$ and $\gamma_T \in \mathbb{R}$ are the Lagrange multipliers associated with the constraints $\boldsymbol{\varphi}_{T,\ell} = 0$ and $\mathbf{1}^T \boldsymbol{\varphi}_T = 1$, respectively. If a solution $(\boldsymbol{\varphi}_T, \boldsymbol{\alpha}_T, \gamma_T)$ to the KKT system (4.8) exists and fulfills $\boldsymbol{\varphi}_T \geq \mathbf{0}$ (primal feasibility) and $\boldsymbol{\alpha}_T \geq \mathbf{0}$

(dual feasibility), then φ_T is in fact a solution to the original problem (4.7). We then assign it to $\varphi_T^{(k+1)}$. Otherwise, the estimate of the active set was incorrect and we use the result of the Riemannian gradient descent stage for $\varphi_T^{(k+1)}$ as a fallback. The entire procedure is shown in Algorithm 2.

Algorithm 2 Solution of the simplex-constrained QP (4.7), the φ -subproblem

Input: $s_T \in \mathbb{R}^L$, $\mathbf{Y}_T \in (\mathcal{T}_{m_T} \mathcal{S})^L$, $\boldsymbol{\lambda}_T \in \mathcal{T}_{m_T} \mathcal{S}$,

Input: $\varphi_T^{(0)} \in \Delta$, $\varepsilon > 0$, $\text{TOL}_1, \text{TOL}_2, \text{TOL}_3 > 0$

Output: approximate solution of (4.7)

```

1: Set  $j \leftarrow 0$ 
2: Set  $\varphi_T^{(0)} \leftarrow \frac{1}{1+\varepsilon L} (\varphi_T^{(0)} + \varepsilon \mathbf{1})$  // recentralize  $\varphi_T^{(0)}$  to the open simplex  $\tilde{\Delta}$ 
3: while  $|\text{grad}_{\tilde{\Delta}} f_T(\varphi_T^{(j)})| > \text{TOL}_1$  and  $\min\{\varphi_{T,\ell}^{(j)} \mid 1 \leq \ell \leq L\} > \text{TOL}_2$  do
4:   Set  $\varphi_T^{(j+1)} \leftarrow \exp_{\varphi_T^{(j)}}(-\boldsymbol{\alpha}_T^{(j+1)} \text{grad}_{\tilde{\Delta}} f_T(\varphi_T^{(j)}))$ 
5:   Set  $j \leftarrow j + 1$ 
6: end while // end of stage 1
7:  $\mathcal{A} = \{1 \leq \ell \leq L \mid \varphi_{T,\ell}^{(j)} > \text{TOL}_3\}$ 
8: Solve the KKT system (4.8) for  $(\varphi_T, \boldsymbol{\alpha}_T, \gamma_T)$ 
9: if  $\boldsymbol{\alpha}_T, \varphi_T \geq \mathbf{0}$  then
10:  return  $\varphi_T$  // solution of (4.7)
11: else
12:  return  $\varphi_T^{(j)}$  // return the result of stage 1 as fallback
13: end if

```

4.2.4. *The \mathbf{m} -Subproblem.* It remains to discuss the update for the variable \mathbf{m} representing the Riemannian center of mass (3.3). Omitting the terms that do not depend on \mathbf{m} as well as the factor $\frac{\rho}{2}$ common to all remaining terms, we obtain

$$\begin{aligned} \text{Minimize}_{\mathbf{m} \in \mathcal{D}\mathcal{G}(\mathcal{T}, \mathcal{S})} \quad & \sum_{T \in \mathcal{T}} |T| \sum_{\ell=1}^L |\exp_{\mathbf{m}_T}(\mathbf{Y}_{T,\ell}^{(k+1)}) - \mathbf{g}_\ell + \boldsymbol{\mu}_{T,\ell}^{(k)}|_2^2 \\ & + \sum_{E \in \mathcal{E}} |E| |\log_{\mathbf{m}_{E_+}}(\mathbf{m}_{E_-}) - \mathbf{X}_E^{(k+1)} + \boldsymbol{\nu}_E^{(k)}|_2^2. \end{aligned}$$

Note, however, that a change of the variable \mathbf{m} always requires a simultaneous update of the tangent vectors $\mathbf{Y}, \mathbf{X}, \boldsymbol{\lambda}, \boldsymbol{\nu}$ to the tangent space of \mathcal{S} at \mathbf{m} . We therefore consider these variables to be dependent on \mathbf{m} and replace them by their parallelly transported counterparts, leading to

$$(4.9) \quad \begin{aligned} \text{Minimize}_{\mathbf{m} \in \mathcal{D}\mathcal{G}(\mathcal{T}, \mathcal{S})} \quad & \sum_{T \in \mathcal{T}} |T| \sum_{\ell=1}^L |\exp_{\mathbf{m}_T}(\mathbf{P}_{\mathbf{m}_T \leftarrow \mathbf{m}_T^{(k)}}(\mathbf{Y}_{T,\ell}^{(k+1)})) - \mathbf{g}_\ell + \boldsymbol{\mu}_{T,\ell}^{(k)}|_2^2 \\ & + \sum_{E \in \mathcal{E}} |E| |\log_{\mathbf{m}_{E_+}}(\mathbf{m}_{E_-}) + \mathbf{P}_{\mathbf{m}_T \leftarrow \mathbf{m}_{E_+}^{(k)}}(-\mathbf{X}_E^{(k+1)} + \boldsymbol{\nu}_E^{(k)})|_2^2. \end{aligned}$$

The explicit representation of the parallel transport was given in (2.1).

Notice that problem (4.9) does not decouple over mesh entities since it contains both a sum over triangles and a sum over edges. It is therefore the most expensive subproblem in the ADMM loop. In the remainder of this subsection, we describe

two approaches to approximately solve (4.9). The first method is a straightforward Riemannian gradient descent scheme with an Armijo backtracking strategy. The second approach is a novel manifold Newton scheme recently devised in Weigl, Schiela, 2024 to find zeros in vector bundles and proven to converge superlinearly. As demonstrated in the experiments in Section 5, this can lead to a significant speedup compared to the gradient descent approach.

We denote the approximate solution of the \mathbf{m} -subproblem (4.9) obtained in either way by $\mathbf{m}^{(k+1)}$. We also update the tangent vectors $\mathbf{Y}^{(k+1)}$, $\mathbf{X}^{(k+1)}$, $\boldsymbol{\nu}^{(k)}$ by their parallelly transported counterparts in their respective tangent spaces pertaining to the new iterate $\mathbf{m}^{(k+1)}$.

Riemannian Gradient Descent for (4.9). For simplicity, we denote the objective in (4.9) by f . The gradient descent scheme is straightforward. It uses the negative Riemannian gradient $\delta\mathbf{m} = -\nabla_{\mathbf{m}}f \in \mathcal{DG}(\mathcal{T}, \mathcal{TS}, \mathbf{m})$ as a descent direction $\delta\mathbf{m}$. The next iterate is then computed via the exponential map as $\exp_{\mathbf{m}}(\tau \delta\mathbf{m})$, where the step size $\tau > 0$ is determined via an Armijo backtracking strategy. Given line-search parameters $\sigma \in (0, 1)$ and $\beta \in (0, 1)$, the step size is chosen as follows: Starting with an initial stepsize τ , we iteratively reduce τ by the factor β until the Armijo condition

$$(4.10) \quad f(\exp_{\mathbf{m}}(\tau \delta\mathbf{m})) \leq f(\mathbf{m}) + \sigma \tau (\nabla_{\mathbf{m}}f, \delta\mathbf{m})$$

is fulfilled. The procedure is summarized in Algorithm 3.

Algorithm 3 Riemannian gradient descent for the \mathbf{m} -subproblem (4.9)

Input: labels $\mathbf{g}_1, \dots, \mathbf{g}_L \in \mathcal{S}$,
Input: Armijo parameters $\sigma \in (0, 1)$, $\beta \in (0, 1)$,
Input: $\mathbf{m} \in \mathcal{DG}(\mathcal{T}, \mathcal{S})$
Input: $\mathbf{Y} \in \mathcal{DG}(\mathcal{T}, \mathcal{TS}, \mathbf{m})^L$, $\mathbf{X} \in \mathcal{DG}(\mathcal{E}, \mathcal{TS}, \mathbf{m})$
Input: $\boldsymbol{\mu} \in \mathcal{DG}(\mathcal{T}, \mathbb{R}^{L \times 3})$, $\boldsymbol{\nu} \in \mathcal{DG}(\mathcal{E}, \mathcal{TS}, \mathbf{m})$
Output: approximate solution of (4.9)

- 1: $\tau \leftarrow 1$
- 2: **while** not converged **do**
- 3: $\delta\mathbf{m} \leftarrow -\nabla_{\mathbf{m}}f(\mathbf{m})$
- 4: $\tau \leftarrow \min\{1, 2\tau\}$
- 5: **while** (4.10) is not fulfilled **do**
- 6: $\tau \leftarrow \beta \tau$
- 7: **end while**
- 8: $\mathbf{m} \leftarrow \exp_{\mathbf{m}}(\tau \delta\mathbf{m})$
- 9: **end while**
- 10: **return** \mathbf{m}

Note that alternatively to starting with the initial stepsize $\tau = 1$ in Algorithm 3, we can also use the previously accepted stepsize τ in the previous ADMM iteration $k - 1$ as an initial guess for the stepsize τ . Either way, the iteration is stopped when a maximum of 10 gradient steps is reached, or when the condition $|\nabla_{\mathbf{m}}f| \leq \max\{10^{-8}, 10^{-0.0025k}\}$ is fulfilled.

Manifold Newton Method for (4.9). As an alternative to the Riemannian gradient descent scheme, we present a novel manifold Newton method. It is based on Weigl, Schiela, 2024 devised to finding zeros in vector bundles. We apply it to the first-order optimality condition of (4.9) w.r.t. the optimization variable $\mathbf{m} \in \mathcal{DG}(\mathcal{T}, \mathcal{S})$, i. e., we seek $\mathbf{m}^* \in \mathcal{DG}(\mathcal{T}, \mathcal{S})$ satisfying

$$(4.11) \quad df(\mathbf{m}^*) = \mathbf{0} \in \mathcal{DG}(\mathcal{T}, \mathcal{T}^*\mathcal{S}, \mathbf{m}^*).$$

Notice that, due to the manifold structure of problem (4.9), the space $\mathcal{DG}(\mathcal{T}, \mathcal{T}^*\mathcal{S}, \mathbf{m}^*)$ depends on the unknown minimizer \mathbf{m}^* .

To formulate Newton's method, we need to derive a suitable Newton equation similar to the classical Newton equation $d^2f(\mathbf{m})\delta\mathbf{m} = -df(\mathbf{m})$ on linear spaces to compute Newton directions $\delta\mathbf{m} \in \mathcal{DG}(\mathcal{T}, \mathcal{TM}, \mathbf{m})$. However, the second derivative $d^2f(\mathbf{m})$ at $\mathbf{m} \in \mathcal{DG}(\mathcal{T}, \mathcal{S})$ is a linear mapping $d^2f(\mathbf{m}): \mathcal{DG}(\mathcal{T}, \mathcal{TS}, \mathbf{m}) \rightarrow \mathcal{T}_{df(\mathbf{m})}(\mathcal{DG}(\mathcal{T}, \mathcal{T}^*\mathcal{S}, \mathbf{m}))$. On the other hand, the right-hand side in Newton's equation $-df(\mathbf{m}) \in \mathcal{DG}(\mathcal{T}, \mathcal{T}^*\mathcal{S}, \mathbf{m})$ is not an element of the same space. This mismatch is resolved by choosing a dual connection $\mathbf{Q}_\ell^*: \mathcal{T}_\ell(\mathcal{DG}(\mathcal{T}, \mathcal{T}^*\mathcal{S}, \mathbf{m})) \rightarrow \mathcal{DG}(\mathcal{T}, \mathcal{T}^*\mathcal{S}, \mathbf{m})$ for $\ell \in \mathcal{DG}(\mathcal{T}, \mathcal{T}^*\mathcal{S}, \mathbf{m})$. That said, we can formulate the manifold Newton equation for (4.11) as

$$(4.12) \quad \mathbf{Q}_{df(\mathbf{m})}^* \circ d^2f(\mathbf{m})\delta\mathbf{m} = -df(\mathbf{m}) \in \mathcal{DG}(\mathcal{T}, \mathcal{T}^*\mathcal{S}, \mathbf{m}).$$

We now describe how to define a dual connection \mathbf{Q}^* and evaluate the first and second derivatives df, d^2f of the objective function f of (4.9) so that we can assemble and solve (4.12). We closely follow the approach proposed in Weigl, Bergmann, Schiela, 2025, Section 5, i. e. we use the Euclidean orthogonal projection from the Riemannian embedding of \mathcal{S} into \mathbb{R}^3 to define a covector back-transport $\mathbb{T}_{\mathbf{m} \leftarrow \cdot}^*$. We then obtain a dual connection \mathbf{Q}^* by differentiating this back-transport.

First, using the pointwise embedding ι of \mathcal{TS} into \mathbb{R}^3 , we can define a pointwise vector transport and corresponding covector back-transport on $\mathcal{T}^*\mathcal{S}$ using orthogonal projections $\mathbf{P}(\mathbf{m}): \mathbb{R}^3 \rightarrow \mathcal{T}_{\mathbf{m}}\mathcal{S}$ for $\mathbf{m} \in \mathcal{S}$. Here, the orthogonal projection is given by $\mathbf{P}(\mathbf{m}) := \mathbf{I}_3 - \mathbf{m}\mathbf{m}^T$, where $\mathbf{I}_3 \in \mathbb{R}^{3 \times 3}$ denotes the identity matrix. We denote the space of linear maps between vector spaces by $L(\cdot, \cdot)$. Setting

$$\mathbb{T}_{\eta \leftarrow \mathbf{m}} := \mathbf{P}(\eta)\iota(\mathbf{m}) \in L(\mathcal{T}_{\mathbf{m}}\mathcal{S}, \mathcal{T}_{\eta}\mathcal{S})$$

for $\eta \in \mathcal{S}$, we obtain a vector transport on the tangent bundle \mathcal{TS} . With this, we can easily construct a vector transport $\mathbb{T}_{\widetilde{\mathbf{m}} \leftarrow \mathbf{m}}: \mathcal{DG}(\mathcal{T}, \mathcal{TS}, \mathbf{m}) \rightarrow \mathcal{DG}(\mathcal{T}, \mathcal{TS}, \widetilde{\mathbf{m}})$ in a triangle-wise fashion by setting

$$(\mathbb{T}_{\widetilde{\mathbf{m}} \leftarrow \mathbf{m}}(\delta\mathbf{m}))_T := \mathbb{T}_{\widetilde{\mathbf{m}}_T \leftarrow \mathbf{m}_T}(\delta\mathbf{m}_T) = \mathbf{P}(\widetilde{\mathbf{m}}_T)\iota(\mathbf{m}_T)\delta\mathbf{m}_T \text{ for all } T \in \mathcal{T},$$

where $\delta\mathbf{m} \in \mathcal{DG}(\mathcal{T}, \mathcal{TS}, \mathbf{m})$, i. e. $\delta\mathbf{m}_T \in \mathcal{T}_{\mathbf{m}_T}\mathcal{S}$.

The corresponding covector back-transport $\mathbb{T}_{\mathbf{m} \leftarrow \cdot}^*$ on the cotangent bundle $\mathcal{DG}(\mathcal{T}, \mathcal{T}^*\mathcal{S}, \mathbf{m})$ is now given by the dual map

$$\langle \mathbb{T}_{\mathbf{m} \leftarrow \widetilde{\mathbf{m}}}^*(\ell), \mathbf{v} \rangle = \langle \ell, \mathbb{T}_{\widetilde{\mathbf{m}} \leftarrow \mathbf{m}}(\mathbf{v}) \rangle \text{ for all } \ell \in \mathcal{DG}(\mathcal{T}, \mathcal{T}^*\mathcal{S}, \widetilde{\mathbf{m}}) \text{ and } \mathbf{v} \in \mathcal{DG}(\mathcal{T}, \mathcal{TS}, \mathbf{m}).$$

We now pass to the dual connection \mathbf{Q}_ℓ^* at $\ell \in \mathcal{DG}(\mathcal{T}, \mathcal{T}^*\mathcal{S}, \mathbf{m})$, obtained by differentiating the covector back-transport $\mathbb{T}_{\mathbf{m} \leftarrow \cdot}^*(\ell)$; see Weigl, Bergmann, Schiela, 2025, Section 5. Specifically, we only need to know $\mathbf{Q}_{df(\mathbf{m})}^* \circ d^2f(\mathbf{m})$. To this end, we apply the techniques from Weigl, Bergmann, Schiela, 2025, Proposition 4.3 in a pointwise fashion. Interpreting the objective f defined in (4.9) as a function

$f: \mathcal{DG}(\mathcal{T}, \mathbb{R}^3) \rightarrow \mathbb{R}$, we denote its derivatives by f' and f'' . Then, the left-hand side in (4.12) can be evaluated as

$$\begin{aligned} \mathbf{Q}_{df(\mathbf{m})}^* d^2 f(\mathbf{m}) \delta \mathbf{m} \\ = f''(\mathbf{m}) \delta \mathbf{m} + f'(\mathbf{m}) (\iota \circ \mathbf{T}_{\mathbf{m} \leftarrow \mathbf{m}})'(\mathbf{m}) \iota(\mathbf{m}) \delta \mathbf{m} \in \mathcal{DG}(\mathcal{T}, \mathcal{T}^* \mathcal{S}, \mathbf{m}), \end{aligned}$$

which corresponds to Weigl, Bergmann, Schiela, 2025, Eq. (22).

It remains to address the Euclidean derivatives f' , f'' of the extended objective function f and $(\mathbf{T}_{\mathbf{m} \leftarrow \mathbf{m}})'$. These can be computed using automatic differentiation tools or using simple calculus. However, the derivatives of the logarithmic terms $\log_{\mathbf{m}_{E_+}}(\mathbf{m}_{E_-})$ in (4.9) require special treatment in case $\mathbf{m}_{E_+} \approx \mathbf{m}_{E_-}$, which is achieved by using the robust formulas (2.5)–(2.7).

We have now defined all components required to assemble the Newton equation (4.12). Although we will be representing the tangent and cotangent vectors in the embedding $\mathcal{S} \subseteq \mathbb{R}^3$, we need to keep in mind the fact that (4.12) is posed on the cotangent space $\mathcal{DG}(\mathcal{T}, \mathcal{T}^* \mathcal{S}, \mathbf{m})$. Thus, we only require the Newton direction $\delta \mathbf{m} \in \mathcal{DG}(\mathcal{T}, \mathcal{T} \mathcal{S}, \mathbf{m})$ to fulfill (4.12) w.r.t. all tangent vectors $\delta \tilde{\mathbf{m}} \in \mathcal{DG}(\mathcal{T}, \mathcal{T} \mathcal{S}, \mathbf{m})$, as opposed to all vectors in $\mathcal{DG}(\mathcal{T}, \mathbb{R}^3)$. Similar to Weigl, Bergmann, Schiela, 2025, Section 6, we address this by constructing a Euclidean-orthonormal basis \mathcal{B} of the embedded tangent space $\mathcal{DG}(\mathcal{T}, \mathcal{T} \mathcal{S}, \mathbf{m})$ and \mathcal{B}^* of the cotangent space $\mathcal{DG}(\mathcal{T}, \mathcal{T}^* \mathcal{S}, \mathbf{m})$. Then, the linear system (4.12) is represented with respect to the chosen bases $\mathcal{B}, \mathcal{B}^*$.

We solve (4.12) using the PETSC implementation of the CG method. We note that the Newton matrix in (4.12) is symmetric but not necessarily positive definite; see Lang, 1999, Chapter XIII, §1. Therefore, the (truncated) CG iteration stops in case a direction of negative curvature is encountered, as described in Nocedal, Wright, 2006, Chapter 7.1. We also exploit the fact that we do not need to solve (4.12) exactly in early ADMM iterations. We therefore require a relative tolerance $\text{RTOL}_{\text{CG}} = \min\{0.1, \|df(\mathbf{m})\|_{\mathcal{DG}(\mathcal{T}, \mathcal{T}^* \mathcal{S}, \mathbf{m})}^{1/2}\}$ to accept a solution $\delta \mathbf{m}$ to the linear system (4.12), with the norm $\|\cdot\|_{\mathcal{DG}(\mathcal{T}, \mathcal{T}^* \mathcal{S}, \mathbf{m})}$ induced by the L^2 -inner product on the cotangent bundle $\mathcal{DG}(\mathcal{T}, \mathcal{T}^* \mathcal{S}, \mathbf{m})$.

This completes the description of the manifold Newton method for the \mathbf{m} -update (4.9). The whole procedure is summarized in Algorithm 4.

Algorithm 4 Manifold Newton method for the \mathbf{m} -subproblem (4.9)

Input: labels $\mathbf{g}_1, \dots, \mathbf{g}_L \in \mathcal{S}$,

Input: $\mathbf{m} \in \mathcal{DG}(\mathcal{T}, \mathcal{S})$

Input: $\mathbf{Y} \in \mathcal{DG}(\mathcal{T}, \mathcal{T} \mathcal{S}, \mathbf{m})^L$, $\mathbf{X} \in \mathcal{DG}(\mathcal{E}, \mathcal{T} \mathcal{S}, \mathbf{m})$

Input: $\boldsymbol{\mu} \in \mathcal{DG}(\mathcal{T}, \mathbb{R}^{L \times 3})$, $\boldsymbol{\nu} \in \mathcal{DG}(\mathcal{E}, \mathcal{T} \mathcal{S}, \mathbf{m})$

Output: approximate solution of (4.9)

- 1: **while** not converged **do**
 - 2: Use truncated CG to compute an inexact Newton direction $\delta \mathbf{m}$ from (4.12)
 - 3: $\mathbf{m} \leftarrow \exp_{\mathbf{m}} \delta \mathbf{m}$
 - 4: **end while**
 - 5: **return** \mathbf{m}
-

We found that in the setting of the ADMM scheme, even a single Newton step per ADMM iteration is sufficient.

4.2.5. *Overall ADMM Scheme.* The overall ADMM scheme for the solution of the label space total variation problem (L-TV) in the form of (4.2) is summarized in Algorithm 5. As was mentioned before, due to the independence of the \mathbf{Y} and \mathbf{X} problems, as well as the φ and \mathbf{m} problems, Algorithm 5 as well as Algorithm 5 can be executed in parallel.

Algorithm 5 ADMM for the label space total variation problem (4.2).

Input: labels $\mathbf{g}_1, \dots, \mathbf{g}_L \in \mathcal{S}$, similarity measure $\mathbf{s} \in \mathcal{DG}(\mathcal{T}, \mathbb{R}^L)$

Input: TV penalty parameter $\beta > 0$, augmentation parameter $\rho > 0$

Input: $\varphi^{(0)} \in \mathcal{DG}(\mathcal{T}, \Delta)$, $\mathbf{m}^{(0)} \in \mathcal{DG}(\mathcal{T}, \mathcal{S})$,

Input: $\mathbf{Y}^{(0)} \in \mathcal{DG}(\mathcal{T}, \mathcal{TS}, \mathbf{m}^{(0)})^L$, $\mathbf{X}^{(0)} \in \mathcal{DG}(\mathcal{E}, \mathcal{TS}, \mathbf{m}^{(0)})$

Output: approximate solution of (4.2)

1: **while** not converged **do**

2: Use a gradient descent scheme to find an approximate minimizer $\mathbf{Y}^{(k+1)}$ of (4.4); see Section 4.2.1.

3: Set $\mathbf{X}^{(k+1)}$ using the soft-thresholding operation (4.6); see Section 4.2.2

4: Set $\varphi^{(k+1)}$ to the solution of (4.7), using Algorithm 2; see Section 4.2.3

5: Use Algorithm 3 (Riemannian gradient descent) or Algorithm 4 (manifold Newton) to find an approximate minimizer $\mathbf{m}^{(k+1)}$ of (4.9); see Section 4.2.4. This also updates $\mathbf{Y}^{(k+1)}$, $\mathbf{X}^{(k+1)}$, $\nu^{(k)}$ via parallel transport.

Update the Lagrange multipliers:

6: $\lambda_T^{(k+1)} \leftarrow \lambda_T^{(k)} + \sum_{\ell=1}^L \varphi_{T,\ell}^{(k+1)} \mathbf{Y}_{T,\ell}^{(k+1)}$ for all $T \in \mathcal{T}$

7: $\mu_{T,\ell}^{(k+1)} \leftarrow \mu_{T,\ell}^{(k)} + \exp_{\mathbf{m}_T^{(k+1)}}(\mathbf{Y}_{T,\ell}^{(k+1)}) - \mathbf{g}_\ell$ for all $T \in \mathcal{T}$ and $\ell = 1, \dots, L$

8: $\nu_E^{(k+1)} \leftarrow \nu_E^{(k)} + \log_{\mathbf{m}_{E_-}^{(k+1)}}(\mathbf{m}_{E_+}^{(k+1)}) - \mathbf{X}_E^{(k+1)}$ for all $E \in \mathcal{E}$

9: **end while**

5. NUMERICAL EXAMPLES

In this section, we compare the solutions of the proposed segmentation problems (A-TV) and (L-TV) for a number of label sets and two different surfaces. For each example, we proceed as follows. We begin with a mesh Γ and add Gaussian noise to the vertex positions. The vertex-dependent variance is chosen as $\sigma^2 = 0.04e^2$ and it scales with the average length e of the edges adjacent to the respective vertex. We then solve (A-TV) using Algorithm 1 and (L-TV) using Algorithm 5.

Since the two variants of total variation penalty are not directly comparable by value, we choose the penalty parameter β independently for each model and example. In each case, we experimentally determine the optimal value β^* in the following way. We solve the assignment problem with $\beta = 0$ for the mesh without noise, which simply amounts to finding the index where $\mathbf{s}_{T,\ell}$ is minimal on each triangle T . We then pick β^* as the value of β that gives the best result in terms of the minimal number of incorrectly labeled triangles, weighted by triangle area. We also show the results for larger and smaller values of β to show the sensitivity to variations of this parameter.

Besides the percentage of correctly labeled triangles (weighted by triangle area), we also report the Rand index RI Hubert, Arabie, 1985; Rand, 1971 to evaluate the quality of the segmentation results. The RI compares two given partitions

$X = \{X_1, \dots, X_k\}$ and $Y = \{Y_1, \dots, Y_r\}$ of a finite set $S = \{s_1, \dots, s_n\}$. It evaluates to $\text{RI} = \frac{a}{b}$, where a is the number of pairs $\{s_i, s_j\}$ that are either in the same subset in both partitions X and Y , or in different subsets in both partitions. Moreover, $b = \binom{n}{2}$ is the total number of pairs.

The assignment function φ takes values in the simplex Δ but not necessarily equal to a vertex. That is, some triangles will be ambiguously labeled, which needs to be resolved both for the purpose of visualization, for the procedure to select the optimal penalty parameter β^* , as well as for the evaluation of both performance metrics. To this end, we simply choose the label with the highest assignment value per triangle in case of the assignment space total variation problem (A-TV). For the label space total variation problem (L-TV), we choose the label g_ℓ with the smallest geodesic distance to the assigned normal $\mathbf{m}(\varphi)_T$. We found this to be a more natural choice in view of the mapping $\varphi_T \mapsto \mathbf{m}(\varphi_T)$ not being injective so that several assignments φ_T yield the same Riemannian center of mass $\mathbf{m}(\varphi_T)$.

The code for the numerical experiments is written in PYTHON using the FENICS finite element library version 2019.1 [Alnæs et al., 2015](#). It was run in parallel using 15 cores on an Intel Quad Xeon CPU@2.6 GHz compute server. The parallelization is based on the built-in MPI support provided by FENICS, which essentially addresses the subproblems in [Algorithms 1](#) and [5](#) by way of domain decomposition. We do not exploit the possible parallel execution of the update steps of \mathbf{Y} and \mathbf{X} and, respectively, φ and \mathbf{m} , as mentioned in [Section 4.2.5](#).

[Table 5.1](#) shows the approximate run time for all experiments in this section, each for the respective optimal value of β^* . In general, the computation time depends on the size of the mesh, the number of labels L , and the TV regularization parameter β . As expected, the more complex label space assignment TV model (L-TV) requires a higher computational effort than the assignment TV model (A-TV). On the other hand, the new Newton method ([Algorithm 4](#)) provides a significant speedup compared to the gradient descent approach ([Algorithm 3](#)) for the \mathbf{m} -update step, which is the main computational bottleneck in the ADMM scheme.

	number of labels L	(A-TV)	(L-TV)	
		Alg. 1	Algs. 5 and 3	Algs. 5 and 4
unit sphere mesh	22	83 s	3400 s	1661 s
fandisk mesh, nonuniform labels	29	272 s	5737 s	3451 s
fandisk mesh, uniform labels	50	138 s	8664 s	4760 s

TABLE 5.1. Approximate run times to solve the (A-TV) and (L-TV) problems for their respective optimal regularization parameters β^* ; see [Tables 5.2](#) to [5.4](#). For the (L-TV) problem solved with the ADMM [Alg. 5](#), we report timings for both gradient descent ([Alg. 3](#)) as well as Newton’s method ([Alg. 4](#)) applied to solve the \mathbf{m} -subproblem.

5.1. Unit Sphere Mesh. The first mesh we consider is a discretization of the unit sphere $\mathcal{S} \subseteq \mathbb{R}^3$ into 4554 triangles. We choose the labels to form an equidistant

partition around the equator, plus the poles, namely

$$(5.1) \quad \mathbf{g}_\ell := \begin{pmatrix} \sin\left(\ell \cdot \frac{2\pi}{20}\right) \\ \cos\left(\ell \cdot \frac{2\pi}{20}\right) \\ 0 \end{pmatrix} \text{ for } \ell = 1, \dots, 20, \quad \mathbf{g}_{21} = \begin{pmatrix} 0 \\ 0 \\ 1 \end{pmatrix} \text{ and } \mathbf{g}_{22} = -\mathbf{g}_{21}.$$

The labels are visualized in Figure 5.1.

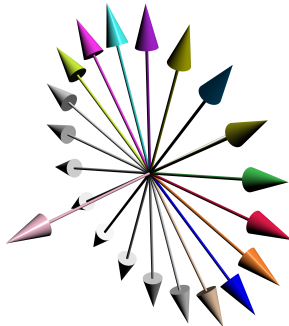


FIGURE 5.1. Visualization of the label set (5.1) for the sphere mesh example (Section 5.1). Labels that are not visible in the corresponding result plots Figure 5.2 are colored in white.

Figure 5.2 shows the resulting assignments for this setup. For each of the two models, we choose $\beta \in \{1/4, 1, 4\} \cdot \beta^*$, where β^* is the optimal parameter choice for the respective model.

For the optimal parameter $\beta_{\text{A-TV}}^*$, the solution of the (A-TV) model uses 21 out of the available 22 labels. However, 6 of the labels are used only on a very small number of triangles and are not visible in Figure 5.2. Overall, 69.4% of all triangles are correctly labeled with a Rand index of 0.953. By contrast, the new (L-TV) uses all 22 labels evenly and achieves an improved correctness of 85.2% and a Rand index of 0.973. Further quantitative results are shown in Table 5.2.

	model	TV weight β	labels used	correctly labeled %	RI
Figure 5.2a	(A-TV)	0.002	22	58.3	0.931
Figure 5.2b	(A-TV)	0.008	21	69.4	0.953
Figure 5.2c	(A-TV)	0.032	9	55.7	0.934
Figure 5.2d	(L-TV)	0.03125	22	83.6	0.972
Figure 5.2e	(L-TV)	0.125	22	85.2	0.973
Figure 5.2f	(L-TV)	0.5	22	81.2	0.964

TABLE 5.2. Quantitative results for the noisy sphere mesh example (Figure 5.2) for different values of the regularization parameter β and the two models. The number of correctly labeled triangles and the Rand index are measured with respect to the ground-truth segmentation given by the original mesh without noise and without regularization ($\beta = 0$).

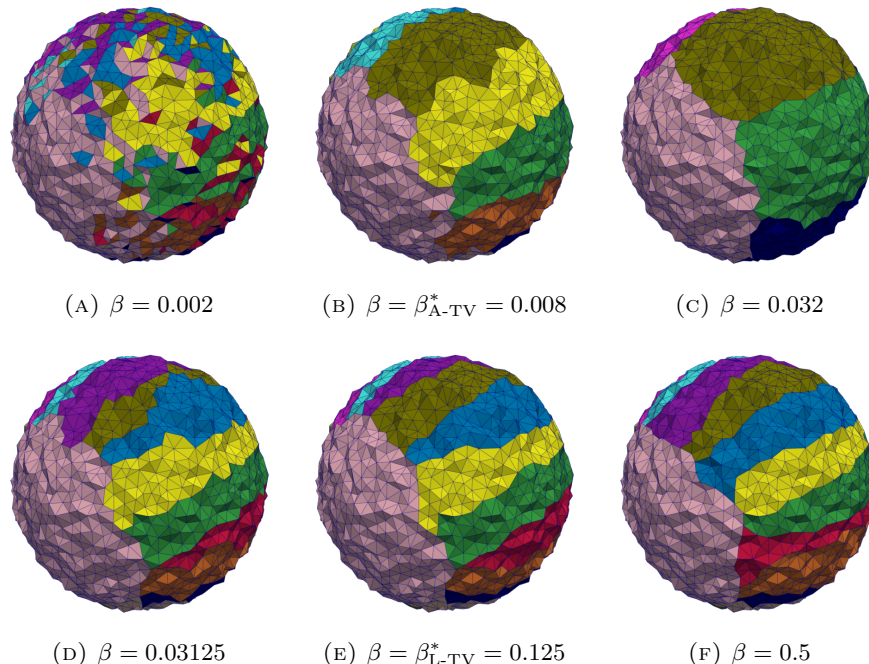


FIGURE 5.2. Assignments for the noisy sphere mesh with different values of β and the label set depicted in Figure 5.1. Triangles are colored according to their assigned label. One of the poles is shown in light pink. Figures 5.2a to 5.2c show the results using (A-TV), while Figures 5.2d to 5.2f show the results using the new (L-TV) model. Quantitative results for these examples are given in Table 5.2.

The sphere mesh together with our choice of labels illustrates that the label space total variation model (L-TV) incurs no additional regularization penalties for “in-between labels”; see also Theorem 3.1 and the discussion there. Therefore, it is able to use all available labels.

A second benefit of the new model is its robustness with respect to the choice of the regularization parameter. In case of too small a regularization parameter (Figure 5.2a), we see that (A-TV) fails to produce segment the mesh in a meaningful way, in contrast to (L-TV). For too large a regularization parameter (Figure 5.2c), the assignment space total variation model (A-TV) does produce meaningful segments, but only uses a subset of the of the available labels, while the label space total variation model (L-TV) still uses all 22. Again, we refer the reader to Table 5.2 for details.

5.2. Fandisk Mesh. Next, we consider the fandisk mesh from Hoppe et al., 1994, which is available at the Wolfram Data Respository Shedelbower, 2022. As above, we added Gaussian noise to the vertex positions. For this example, we consider two different label sets. The first label set has 29 labels and they are chosen to represent the normals occurring on the round parts of the fandisk mesh well. The aim is to allow for a finer segmentation of the mesh on said parts. By contrast, the

second label set consists of 50 labels that are distributed uniformly on the sphere. We obtain this label set using a Fibonacci lattice; see [González, 2009](#). The label sets are visualized in [Figure 5.3](#).

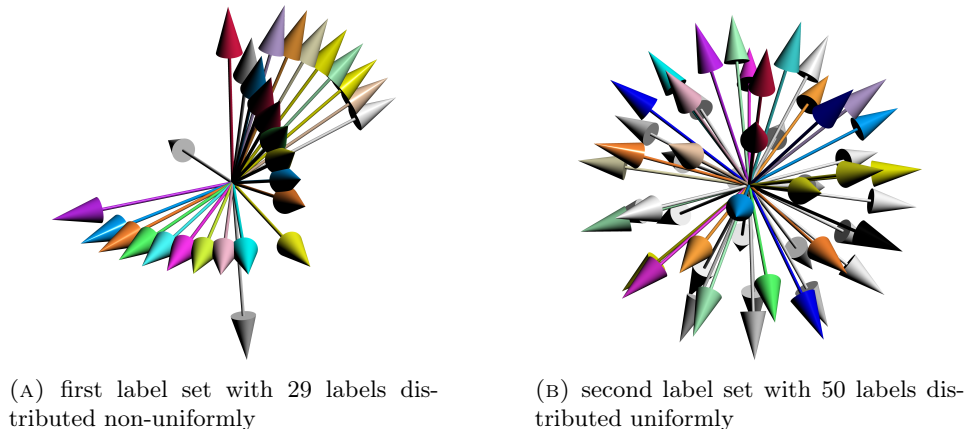


FIGURE 5.3. Visualization of the two label sets for the fandisk mesh example ([Section 5.2](#)). Labels that are not visible in the corresponding result plots [Figures 5.4](#) and [5.5](#) are colored in white.

The results for the first label set are shown in [Figure 5.4](#). For each of the two models, we choose $\beta \in \{1/2, 1, 2\} \cdot \beta^*$, where β^* is the optimal parameter choice for the respective model.

For the optimal parameter $\beta_{\text{A-TV}}^*$, the solution of the (A-TV) model uses 26 out of the available 29 labels and correctly labels 89.6% of the triangles with a Rand index of 0.989. The new (L-TV) uses 27 labels and achieves a correctness of 91.4% with a Rand index of 0.987. Further quantitative results are shown in [Table 5.3](#).

	model	TV weight β	labels used	correctly labeled %	RI
Figure 5.4a	(A-TV)	0.004	29	81.7	0.975
Figure 5.4b	(A-TV)	0.008	26	89.6	0.989
Figure 5.4c	(A-TV)	0.016	15	85.5	0.981
Figure 5.4d	(L-TV)	0.02	29	81.9	0.976
Figure 5.4e	(L-TV)	0.04	27	91.4	0.987
Figure 5.4f	(L-TV)	0.08	27	85.4	0.980

TABLE 5.3. Quantitative results for the noisy fandisk mesh example ([Figure 5.4](#)) with the first label set 29 labels for different values of the regularization parameter β and the two models. The number of correctly labeled triangles and the Rand index are measured with respect to the ground-truth segmentation given by the original mesh without noise and without regularization ($\beta = 0$).

We observe that the (L-TV) is able to assign a more detailed segmentation of the round parts in the front both for the optimal parameter $\beta_{\text{L-TV}}^*$ and also for

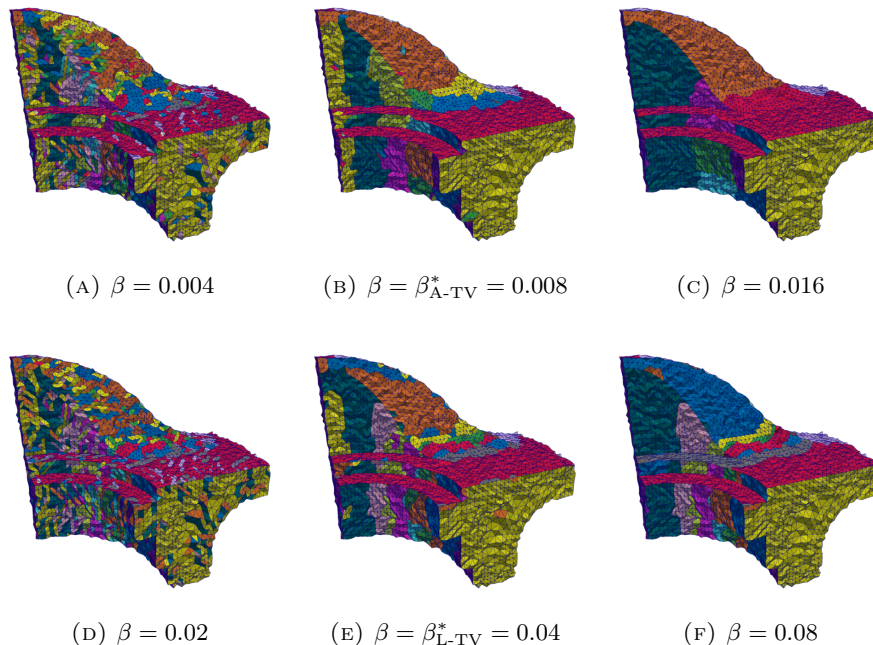


FIGURE 5.4. Assignments for the noisy fan-disk mesh with the first label set of 29 labels (Figure 5.3a) and different values of β . Triangles are colored according to their assigned label. Figures 5.4a to 5.4c show the results using (A-TV), while Figures 5.4d to 5.4f show the results using (L-TV). Quantitative results for these examples are given in Table 5.3.

$2\beta_{L-TV}^*$. This shows that for this setup, the (L-TV) is again more robust against choosing a regularization parameter β that is too large. Both models fail to produce a meaningful segmentation when the regularization parameter is $\beta^*/2$.

The results for the second label set are shown in Figure 5.5.

In this case, the (A-TV) model uses 26 of the available 50 labels and correctly labels 86.8% of the mesh with a Rand index of 0.978, while the (L-TV) model uses 35 labels and correctly labels 85.2% of the mesh with a Rand index of 0.977. Further quantitative results are shown in Table 5.4.

We see that (L-TV) is having difficulties in removing the noise near the sharp boundaries between labels, even for higher values of the regularization parameter β . On the other hand, the (L-TV) is able to more precisely recover the round parts of the original mesh and remove the noise.

6. CONCLUSION

In this paper, we have compared two variational models for the segmentation of triangulated surfaces based on the normal vector field as the governing feature. The classical assignment space total variation model (A-TV) penalizes the total variation of the assignment function directly. Every transition from one vertex in the assignment simplex to another is equally penalized with a value of 2. By

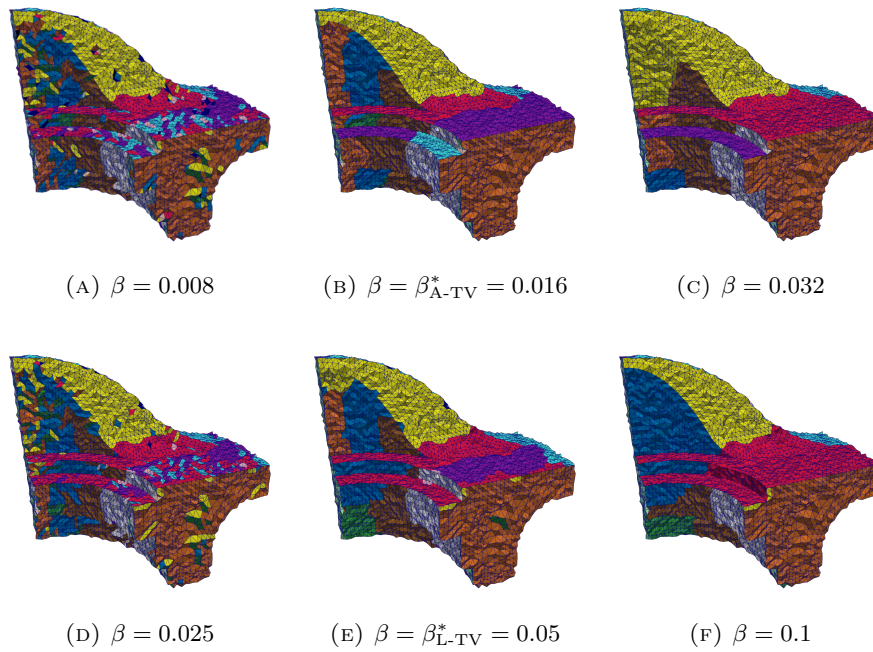


FIGURE 5.5. Assignments for the noisy fan disk mesh with the second label set of 50 uniformly distributed labels (Figure 5.3b) with different values of β . Triangles are colored according to their assigned label. Figures 5.5a to 5.5c show the results using (A-TV), while Figures 5.5d to 5.5f show the results using (L-TV). Quantitative results for these examples are given in Table 5.4.

	model	TV weight β	labels used	correctly labeled %	RI
Figure 5.5a	(A-TV)	0.008	50	73.3	0.955
Figure 5.5b	(A-TV)	0.016	26	86.8	0.978
Figure 5.5c	(A-TV)	0.032	15	79.6	0.969
Figure 5.5d	(L-TV)	0.025	46	75.3	0.957
Figure 5.5e	(L-TV)	0.05	35	85.2	0.977
Figure 5.5f	(L-TV)	0.1	32	74.3	0.959

TABLE 5.4. Quantitative results for the noisy fan disk mesh example (Figure 5.5) with the second label set of 50 uniformly distributed labels for different values of the regularization parameter β and the two models. The number of correctly labeled triangles and the Rand index are measured with respect to the ground-truth segmentation given by the original mesh without noise and without regularization ($\beta = 0$).

contrast, the label space total variation model (L-TV) penalizes the total variation of the normal vector represented by the assignment function in the label space \mathcal{S} .

Consequently, every transition from one vertex in the assignment simplex to another has a cost proportional to the geodesic distance between the corresponding labels on the sphere.

While (L-TV) appears equally natural, it is computationally significantly more challenging to solve than (A-TV). This additional complexity needs to be taken into account when selecting between the two models for a given application. The added complexity is due to the fact that the labels are situated in a nonlinear space (the sphere), and the evaluation of their mixture requires a Riemannian center of mass problem to be solved on each triangle as part of the optimization process. In order to mitigate the computational overhead, we proposed a novel manifold Newton method for the subproblem arising from the Riemannian center of mass problem in the ADMM loop. Numerical experiments show that this speeds up the overall optimization significantly compared to a gradient descent approach. Still, the (L-TV) remains computationally more expensive than (A-TV) when solved using ADMM.

We observed that (A-TV) does not necessarily use all available labels, especially for large values of the regularization parameter. In particular, this can be observed in regions of constant curvature and multiple labels available for this region. In contrast, the proposed model (L-TV) utilizes more of the available labels. It also turns out to be more robust w.r.t. the choice of the regularization parameter β .

REFERENCES

- Alnæs, M.; J. Blechta; J. Hake; A. Johansson; B. Kehlet; A. Logg; C. Richardson; J. Ring; M. E. Rognes; G. N. Wells (2015). “The FEniCS project version 1.5”. *Archive of Numerical Software* 3.100, pp. 9–23. DOI: [10.11588/ans.2015.100.20553](https://doi.org/10.11588/ans.2015.100.20553).
- Åström, F.; S. Petra; B. Schmitzer; C. Schnörr (2017). “Image labeling by assignment”. *Journal of Mathematical Imaging and Vision* 58.2, pp. 211–238. DOI: [10.1007/s10851-016-0702-4](https://doi.org/10.1007/s10851-016-0702-4).
- Bae, E.; J. Yuan; X.-C. Tai; Y. Boykov (2014). “A fast continuous max-flow approach to non-convex multi-labeling problems”. *Efficient Algorithms for Global Optimization Methods in Computer Vision*. Springer Berlin Heidelberg, pp. 134–154. DOI: [10.1007/978-3-642-54774-4_7](https://doi.org/10.1007/978-3-642-54774-4_7).
- Bergmann, R.; M. Herrmann; R. Herzog; S. Schmidt; J. Vidal-Núñez (2020a). “Discrete total variation of the normal vector field as shape prior with applications in geometric inverse problems”. *Inverse Problems* 36.5, p. 054003. DOI: [10.1088/1361-6420/ab6d5c](https://doi.org/10.1088/1361-6420/ab6d5c). arXiv: [1908.07916](https://arxiv.org/abs/1908.07916).
- Bergmann, R.; M. Herrmann; R. Herzog; S. Schmidt; J. Vidal-Núñez (2020b). “Total variation of the normal vector field as shape prior”. *Inverse Problems* 36.5, p. 054004. DOI: [10.1088/1361-6420/ab6d5b](https://doi.org/10.1088/1361-6420/ab6d5b). arXiv: [1902.07240](https://arxiv.org/abs/1902.07240).
- Boumal, N. (2023). *An Introduction to Optimization on Smooth Manifolds*. Cambridge University Press. DOI: [10.1017/9781009166164](https://doi.org/10.1017/9781009166164). URL: <https://www.nicolasboumal.net/book>.
- Boyd, S.; N. Parikh; E. Chu; B. Peleato; J. Eckstein (2010). “Distributed optimization and statistical learning via the alternating direction method of multipliers”. *Foundations and Trends in Machine Learning* 3.1, pp. 1–122. DOI: [10.1561/22000000016](https://doi.org/10.1561/22000000016).

- Chambolle, A.; T. Pock (2011). “A first-order primal-dual algorithm for convex problems with applications to imaging”. *Journal of Mathematical Imaging and Vision* 40.1, pp. 120–145. DOI: [10.1007/s10851-010-0251-1](https://doi.org/10.1007/s10851-010-0251-1).
- Charles, R. Q.; H. Su; M. Kaichun; L. J. Guibas (2017). “PointNet: deep learning on point sets for 3D classification and segmentation”. *2017 IEEE Conference on Computer Vision and Pattern Recognition (CVPR)*. IEEE, pp. 77–85. DOI: [10.1109/cvpr.2017.16](https://doi.org/10.1109/cvpr.2017.16).
- Cohen-Steiner, D.; P. Alliez; M. Desbrun (2004). “Variational shape approximation”. *ACM Transactions on Graphics* 23.3, pp. 905–914. DOI: [10.1145/1015706.1015817](https://doi.org/10.1145/1015706.1015817).
- Gauthier, S.; W. Puech; R. Bénéière; G. Subsol (2017). “Digitized 3D mesh segmentation based on curvature analysis”. *Electronic Imaging* 29.20, pp. 33–38. DOI: [10.2352/issn.2470-1173.2017.20.3dipm-005](https://doi.org/10.2352/issn.2470-1173.2017.20.3dipm-005).
- Goldstein, T.; S. Osher (2009). “The split Bregman method for L_1 -regularized problems”. *SIAM Journal on Imaging Sciences* 2.2, pp. 323–343. DOI: [10.1137/080725891](https://doi.org/10.1137/080725891).
- González, A. (2009). “Measurement of areas on a sphere using Fibonacci and latitude-longitude lattices”. *Mathematical Geosciences* 42.1, pp. 49–64. DOI: [10.1007/s11004-009-9257-x](https://doi.org/10.1007/s11004-009-9257-x).
- Goto, J.; H. Sato (2021). “Approximated logarithmic maps on Riemannian manifolds and their applications”. *JSIAM Letters* 13, pp. 17–20. DOI: [10.14495/jsiaml.13.17](https://doi.org/10.14495/jsiaml.13.17).
- Hanocka, R.; A. Hertz; N. Fish; R. Giryes; S. Fleishman; D. Cohen-Or (2019). “MeshCNN: a network with an edge”. *ACM Transactions on Graphics* 38.4, pp. 1–12. DOI: [10.1145/3306346.3322959](https://doi.org/10.1145/3306346.3322959).
- He, Y.; M. Yousuff Hussaini; J. Ma; B. Shafei; G. Steidl (2012). “A new fuzzy c-means method with total variation regularization for segmentation of images with noisy and incomplete data”. *Pattern Recognition* 45.9, pp. 3463–3471. DOI: [10.1016/j.patcog.2012.03.009](https://doi.org/10.1016/j.patcog.2012.03.009).
- Hoppe, H.; T. DeRose; T. Duchamp; M. Halstead; H. Jin; J. McDonald; J. Schweitzer; W. Stuetzle (1994). “Piecewise smooth surface reconstruction”. *Proceedings of the 21st Annual Conference on Computer Graphics and Interactive Techniques - SIGGRAPH '94*. ACM Press, pp. 295–302. DOI: [10.1145/192161.192233](https://doi.org/10.1145/192161.192233).
- Hubert, L.; P. Arabie (1985). “Comparing partitions”. *Journal of Classification* 2.1, pp. 193–218. DOI: [10.1007/bf01908075](https://doi.org/10.1007/bf01908075).
- Hwan Kim, D.; I. Dong Yun; S. Uk Lee (2006). “Boundary-trimmed 3D triangular mesh segmentation based on iterative merging strategy”. *Pattern Recognition* 39.5, pp. 827–838. DOI: [10.1016/j.patcog.2005.11.022](https://doi.org/10.1016/j.patcog.2005.11.022).
- Karcher, H. (1977). “Riemannian center of mass and mollifier smoothing”. *Communications on Pure and Applied Mathematics* 30.5, pp. 509–541. DOI: [10.1002/cpa.3160300502](https://doi.org/10.1002/cpa.3160300502).
- Lang, S. (1999). *Fundamentals of Differential Geometry*. Springer New York. DOI: [10.1007/978-1-4612-0541-8](https://doi.org/10.1007/978-1-4612-0541-8).
- Lellmann, J.; J. Kappes; J. Yuan; F. Becker; C. Schnörr (2009). “Convex multi-class image labeling by simplex-constrained total variation”. *Scale Space and Variational Methods in Computer Vision*. Ed. by X.-C. Tai; K. Mørken; M. Lysaker; K.-A. Lie. Vol. 5567. Lecture Notes in Computer Science. Springer Berlin Heidelberg, pp. 150–162. DOI: [10.1007/978-3-642-02256-2_13](https://doi.org/10.1007/978-3-642-02256-2_13).

- Lellmann, J.; C. Schnörr (2011). “Continuous multiclass labeling approaches and algorithms”. *SIAM Journal on Imaging Sciences* 4.4, pp. 1049–1096. DOI: [10.1137/100805844](https://doi.org/10.1137/100805844).
- Lellmann, J.; E. Strelakovsky; S. Koetter; D. Cremers (2013). “Total variation regularization for functions with values in a manifold”. *2013 IEEE International Conference on Computer Vision*, pp. 2944–2951. DOI: [10.1109/ICCV.2013.366](https://doi.org/10.1109/ICCV.2013.366).
- Li, Q.; D. McKenzie; W. Yin (2021). *From the simplex to the sphere: faster constrained optimization using the Hadamard parametrization*. arXiv: [2112.05273](https://arxiv.org/abs/2112.05273).
- Mumford, D.; J. Shah (1989). “Optimal approximations by piecewise smooth functions and associated variational problems”. *Communications on Pure and Applied Mathematics* 42.5, pp. 577–685. DOI: [10.1002/cpa.3160420503](https://doi.org/10.1002/cpa.3160420503).
- Nabi, H.; A. Douik (2016). “An extended Mumford-Shah model for shape partitioning”. *International Journal of Signal and Imaging Systems Engineering* 9.4/5, p. 226. DOI: [10.1504/ijwise.2016.078263](https://doi.org/10.1504/ijwise.2016.078263).
- Nocedal, J.; S. J. Wright (2006). *Numerical Optimization*. 2nd ed. New York: Springer. DOI: [10.1007/978-0-387-40065-5](https://doi.org/10.1007/978-0-387-40065-5).
- Pock, T.; D. Cremers; H. Bischof; A. Chambolle (2009). “An algorithm for minimizing the Mumford-Shah functional”. *2009 IEEE 12th International Conference on Computer Vision*. IEEE, pp. 1133–1140. DOI: [10.1109/iccv.2009.5459348](https://doi.org/10.1109/iccv.2009.5459348).
- Rand, W. M. (1971). “Objective criteria for the evaluation of clustering methods”. *Journal of the American Statistical Association* 66.336, pp. 846–850. DOI: [10.1080/01621459.1971.10482356](https://doi.org/10.1080/01621459.1971.10482356).
- Shedelbower, A. (2022). *Sample 3D Model: Fan Disk*. Wolfram Data Repository. URL: <https://datarepository.wolframcloud.com/resources/Sample-3D-Model-Fan-Disk/> (visited on 05/17/2023).
- Stellato, B.; G. Banjac; P. Goulart; A. Bemporad; S. Boyd (2020). “OSQP: an operator splitting solver for quadratic programs”. *Mathematical Programming Computation* 12.4, pp. 637–672. DOI: [10.1007/s12532-020-00179-2](https://doi.org/10.1007/s12532-020-00179-2).
- Sun, Z.; R. Harik; S. Baek (2018). “Mesh segmentation via geodesic curvature flow”. *Computer-Aided Design and Applications* 15.5, pp. 677–683. DOI: [10.1080/16864360.2018.1441235](https://doi.org/10.1080/16864360.2018.1441235).
- Wang, J.; Z. Yu (2011). “Surface feature based mesh segmentation”. *Computers & Graphics* 35.3, pp. 661–667. DOI: [10.1016/j.cag.2011.03.016](https://doi.org/10.1016/j.cag.2011.03.016).
- Wang, W.; M. Á. Carreira-Perpiñán (2013). *Projection onto the probability simplex: an efficient algorithm with a simple proof, and an application*. arXiv: [1309.1541](https://arxiv.org/abs/1309.1541).
- Weigl, L.; R. Bergmann; A. Schiela (2025). *Newton’s method for nonlinear mappings into vector bundles. Part II: application to variational problems*. arXiv: [2507.13836v1](https://arxiv.org/abs/2507.13836v1).
- Weigl, L.; A. Schiela (2024). *Newton’s method for nonlinear mappings into vector bundles*. arXiv: [2404.04073v2](https://arxiv.org/abs/2404.04073v2).
- Wu, C.; J. Zhang; Y. Duan; X.-C. Tai (2012). “Augmented Lagrangian method for total variation based image restoration and segmentation over triangulated surfaces”. *Journal of Scientific Computing* 50.1, pp. 145–166. DOI: [10.1007/s10915-011-9477-3](https://doi.org/10.1007/s10915-011-9477-3).
- Yamauchi, H.; S. Gumhold; R. Zayer; H.-P. Seidel (2005). “Mesh segmentation driven by Gaussian curvature”. *The Visual Computer* 21.8–10, pp. 659–668. DOI: [10.1007/s00371-005-0319-x](https://doi.org/10.1007/s00371-005-0319-x).

- Yan, D.-M.; W. Wang; Y. Liu; Z. Yang (2012). “Variational mesh segmentation via quadric surface fitting”. *Computer-Aided Design* 44.11, pp. 1072–1082. DOI: [10.1016/j.cad.2012.04.005](https://doi.org/10.1016/j.cad.2012.04.005).
- Yuan, J.; E. Bae; X.-C. Tai (2010). “A study on continuous max-flow and min-cut approaches”. *2010 IEEE Computer Society Conference on Computer Vision and Pattern Recognition*. IEEE, pp. 2217–2224. DOI: [10.1109/cvpr.2010.5539903](https://doi.org/10.1109/cvpr.2010.5539903).
- Yuan, J.; E. Bae; X.-C. Tai; Y. Boykov (2010). “A continuous max-flow approach to Potts model”. *Computer Vision – ECCV 2010*. Ed. by K. Daniilidis; P. Maragos; N. Paragios. Springer Berlin Heidelberg, pp. 379–392. DOI: [10.1007/978-3-642-15567-3_28](https://doi.org/10.1007/978-3-642-15567-3_28).
- Zhang, H.; C. Wu; J. Deng; Z. Liu; Y. Yang (2017). “A new two-stage mesh surface segmentation method”. *The Visual Computer* 34.11, pp. 1597–1615. DOI: [10.1007/s00371-017-1434-1](https://doi.org/10.1007/s00371-017-1434-1).
- Zhang, J.; J. Zheng; C. Wu; J. Cai (2012). “Variational mesh decomposition”. *ACM Transactions on Graphics* 31.3, pp. 1–14. DOI: [10.1145/2167076.2167079](https://doi.org/10.1145/2167076.2167079).
- (M. Weiß) INTERDISCIPLINARY CENTER FOR SCIENTIFIC COMPUTING, HEIDELBERG UNIVERSITY, 69120 HEIDELBERG, GERMANY
Email address: manuel.weiss@iwr.uni-heidelberg.de
URL: <https://scoop.iwr.uni-heidelberg.de>
- (L. Baumgärtner) INSTITUT FÜR MATHEMATIK, HUMBOLDT UNIVERSITY OF BERLIN, 10099 BERLIN, GERMANY
Email address: lukas.baumgaertner@hu-berlin.de
URL: <https://www.mathematik.hu-berlin.de/en/people/mem-vz/1693318>
- (L. Weigl) UNIVERSITÄT BAYREUTH, UNIVERSITÄTSSTRASSE 30, 95447 BAYREUTH, GERMANY
Email address: laura.weigl@uni-bayreuth.de
URL: <https://num.math.uni-bayreuth.de/de/team/laura-weigl>
- (R. Bergmann) NORWEGIAN UNIVERSITY OF SCIENCE AND TECHNOLOGY, DEPARTMENT OF MATHEMATICAL SCIENCES, NO-7041 TRONDHEIM, NORWAY
Email address: ronny.bergmann@ntnu.no
URL: <https://www.ntnu.edu/employees/ronny.bergmann>
- (S. Schmidt) UNIVERSITY OF TRIER, UNIVERSITÄTSRING 15, 54296 TRIER, GERMANY
Email address: s.schmidt@uni-trier.de
URL: <https://www.math.uni-trier.de/~schmidt>
- (R. Herzog) INTERDISCIPLINARY CENTER FOR SCIENTIFIC COMPUTING, HEIDELBERG UNIVERSITY, 69120 HEIDELBERG, GERMANY
Email address: roland.herzog@iwr.uni-heidelberg.de
URL: <https://scoop.iwr.uni-heidelberg.de>